A novel technique for phased array receivers using an economic sampling scheme

Rodrigo Blanco Moro

Thesis submitted to the Faculty of the
Virginia Polytechnic Institute and State University
in partial fulfillment of the requirements for the degree of

Master of Science
in
Electrical Engineering

Majid Manteghi, Chair
Kwan-Jin Koh
J. Michael Ruohoniemi

July 15, 2013
Blacksburg, Virginia

Keywords: Antennas, Bandwidth enhancement, Phased array, Sampling scheme, Tapering

VIRGINIA POLYTECHNIC INSTITUTE AND STATE UNIVERSITY

Abstract

Bradley Department of Electrical Engineering

Master of Science

A novel technique for phased array receivers using an economic sampling scheme

by Rodrigo Blanco Moro

Phased array systems present desirable antenna features like beam steering and high gain. However, due to their high cost, civilian applications cannot generally afford them, restricting their usage to military. Hardware involved in phased array systems is expensive and the number of devices is high, since there is usually one device of each kind (filter, amplifier, shifter..) for each individual antenna. Alternative techniques, mainly based on TDMA, have been developed looking for lowering the number of elements in the system. However, these approaches increase the system bandwidth, multiplying it by a factor of N (Number of antennas), as they use redundant information.

In this thesis, a novel phased receiver, based on an economic sampling scheme is proposed. All the elements in an array receive a common information (signal amplitude) and a unique information (relative delay between elements). The idea is to sample only the information required to reconstruct the transmitted signal and discard the redundant one. This idea is achieved by sampling just one antenna during each RF cycle and then gathering all the information taking in account the relative delay between different antenna elements.

The proposed technique is mathematically proved and validated by simulation. As a first approach, the equation for the received signal in the frequency domain is derived for a linear array. The radiation pattern and the received signals are simulated for equally spaced planar and linear arrays. Bandwidth signal transmission is demonstrated and tapering effects are shown. After that, the proposed technique is expanded for arbitrary structures and the resulting system bandwidth is enhanced by using different sampling order sequences.

"Progress is the only option when one thinks big. It is only possible to move forward when one looks away."

José Ortega y Gasset

(Sólo cabe progresar cuando se piensa en grande. Sólo es posible avanzar cuando se mira lejos)

Acknowledgements

It is a pleasure for me to dedicate this page to the people that have made possible this work. First of all, I would like to thank my advisor, Dr. Majid Manteghi, for taking me as his student and giving me the opportunity to work in this amazing project. His advise, comments and guidance have been extremely valuable for my research. I would also like to thank Dr. J. Michael Ruohoniemi and Dr. Kwang-Jin Koh for their time in serving on my advisory committee, as well as their constructive suggestions to improve my thesis.

My gratitude also goes to the Institute for Critical Technology and Applied Science (ICTAS) at Virginia Tech, and specially to Dr. Jeffrey Reed, for his financial support.

I would also like to have some words to the Virginia Tech Antenna Group members. I have been lucky to be surrounded by amazing people and I would like to thank Reza for his considerably large amount of help with my research, Carlos for his estimable support, Shyam for his infinite patience and priceless collaboration with my English documents and Mohsen, the greatest lab senior.

It would be completely unfair to forget about my Spanish friends. I would need a whole chapter to mention all of them, but I would like to thank Humber, Roberto, Mario, Marta, Marcos, Cardalda, Dani and many others, four thousand miles away from Blacksburg, but as close as if I were in Oviedo.

Finally, I would like to give my family the special recognition they deserve. There is no way to write how important it is for me the endless and unconditional love I have received and no word that describes how grateful I am to my parents and grandparents, because I would never be able to reach this point without them.

Contents

List of Figures

List of Tables

Abbreviations

ADC	**A**nalog to **D**igital **C**onverter
AF	**A**rray **F**actor
BW	**B**and**W**idth
DSB	**D**ouble **S**ide **B**and
DSP	**D**igital **S**ignal **P**rocessor
FDMA	**F**requency **D**ivision **M**ultiple **A**ccess
GA	**G**enetic **A**lgorithm
IF	**I**ntermediate **F**requency
LNA	**L**ow **N**oise **A**mplifier
LO	**L**ocal **O**scillator
PLL	**P**hase-**L**ocked **L**oop
RF	**R**adio **F**requency
SLL	**S**ide**L**obe **L**evel
TDMA	**T**ime **D**ivision **M**ultiple **A**ccess

Notation

Variable	Description	Unit
	Signals	
$f(t)$	Composed signal	V/m
$f_{n,i}(t)$	Received signal at n^{th} antenna	V/m
$f_n(t)$	Signal at n^{th} antenna after alignment	V/m
$f_0(t)$	Phase reference signal	V/m
$s(t)$	General switching signal	
$s_n(t)$	Switching signal for n^{th} antenna	
$\Pi(t)$	Rectangular pulse, centered at origin and unit width	
$\Gamma(x)$	Heaviside step function	
	Indexing	
m	Indexing for harmonic number	
n	Indexing for antenna number	
	Electromagnetics	
λ	wavelength	m
k	Wave number	1/m
β	Phase constant	rad/m
C	Light velocity in free space	m/s
f	Frequency	Hz
ω	Angular pulsation	rad/s
$\vec{r}_n$	Space point location	m

	Array description	
N	Array number of elements	
(θ_0, φ_0)	Array scanned direction	deg
(θ_i, φ_i)	Incoming wave direction	deg
d	Space between elements (constant spacing)	m
$\vec{r}_n'$	Space point location	m
R	Array layout coordinates in matrix form	m/s
A_n	Complex excitation of nth element	V
a_n	Amplitude excitation of nth element	V
α_n	Phase excitation of nth element	rad
ψ	Array space domain	
	Sampling technique	
t_s	Single element sampling period	s
T_s	Aperture sampling period	s
ω_s	Single element sampling rate	rad/s
Ω_s	Aperture sampling rate	rad/s
$\Delta t_{n-1,n}$	Time lapse between n-1th and n th antenna	s
i_n	Waited / Loss cycles before sampling nth antenna	
	Tapering	
σ	Standard deviation for Gaussian distribution tapering	
$\tilde{n}$	Number of sidelobes without $1/u$ falloff	

To my parents and grandparents

my source of inspiration, my motivation to do my best

Chapter 1

Introduction

Contents

1.1 Motivation

Phased array antennas have been widely used when a high gain and electronically steered antenna is necessitated. Their traditional field of application is military, especially radar [1], since the system cost is generally not affordable for civilian applications. Later fields of applications include astronomy [2], satellite communications [3, 4], ultrasonic [5, 6] or cellular base stations [7, 8].

A traditional phased array includes a variable phase shifter before (for transmission) or after (for reception) each antenna which is configured in such a way that the signals from all elements add in phase for a certain angle. This process, known as beamforming [9], can be done in the analog domain, the digital domain or using hybrid techniques [10].

- **Analog Domain**: Beamforming in the analog domain uses analog shifters, which are generally lossy and expensive. In addition, a phase shifter, as well as an amplifier, is needed for each antenna, so the system cost increases proportionally to the number of antennas.
- **Digital domain**: Beamforming in the digital domain is done using a DSP (Digital Signal Processor) or similar, which is conected to an ADC (Analog to Digital

Converter) input. Digital phased arrays are cheaper since they do not use phase shifters, however, as the number of elements and frequency increases, it becomes a difficult challenge to process all the data.

- **Hybrid techniques**: The phase shift is generated at the local oscillator of each RF path and the signals are added at the IF or baseband. As negative points, hybrid techniques require multiple PLL's as well as extra components to control them.

Phased array elevated cost is mainly caused by the elevated number of components that the system needs. As a result, it becomes interesting to look for alternatives which reduce the number of devices. For that purpose TDMA (Time Division Multiple Access) and FDMA (Frequency Division Multiply Access) can be used. To the best of the author's knowledge, first appareance of TDMA/FDMA is [11].

Traditionally, TDMA has been preferred to FDMA, and multiple topologies have been proposed using digital phased arrays. Spacial MultIplexing of Local Elements (SMILE) which allows the system to reduce the number of components is proposed in [12, 13]. SMILE is based on TDMA and the multiplexing is done using a PIN diode [12] or a low noise amplifier [13]. A hardware implementation is shown in [14], which uses a high speed switch after the front ends to perform the multiplexing.

The commented approaches succeed in reducing the number of devices in the system. However, they integrate the information from the N antennas into a common RF path, yielding a bandwidth N times larger than the original signal bandwidth. For large arrays, the required bandwidth is increased one or even two orders of magnitude only to process much redundant information, as the amplitude received at each antenna is common to all the elements. As a result, the system may get unnecessarily complex due to the high computational cost.

The technique presented in this thesis allows lowering the system cost by reducing the number of RF paths down to one and at the same time, keep the original signal bandwidth as a result of not sampling redundant information. By sampling only one antenna each RF cycle (as explained in Chapter 3) and taking in account the time propagation difference between the array elements, the receiver does not have to deal with redundant information and all benefits from phased array antennas (steerable beam, high gain) can be maintained.

1.2 Objectives

The objective is to design a simplified phased array receiver, as powerful as the traditional approach one, which must fulfill the following requirements:

- The receiver must maintain phased array characteristics in terms of steerable beam and high gain.
- System cost must be considerably less expensive.
- The receiver must be suitable for civilian usage.

1.3 Thesis organization

This thesis is divided in 6 chapters, including this one as an introduction, and two appendices. Each chapter can be described as follows:

- Chapter 1 acts as an introduction to the thesis in terms of motivation, objectives and structure.
- Chapter 2 introduces phased array theory, focusing in the constructive interference in time domain and array factor for linear arrays, since both results are used in later chapters to prove the equivalence between the proposed technique and the traditional phased array approach. Different beamforming techniques are also explained.
- Chapter 3 explains the proposed technique and proves it mathematically and validates it by simulating canonical structures like linear and planar arrays. The system bandwidth limit is introduced and the transmission of real signals (carrying data signals) is simulated.
- Chapter 4 shows the effect of tapering. Three different tapering techniques have been considered: Gaussian, Dolph-Chebyshev and Taylor N-bar.
- Chapter 5 focuses on the bandwidth enhancement. A formulation for arbitrary arrays is introduced and used to describe generic order sampling. The effect of sampling order is studied and optimized using backtracking and a genetic algorithm. Maximum delay sampling is explained and its optimality is illustrated. Finally, aperiodic sampling order is described and simulated

- Chapter 6 gathers the most important thesis concepts as well as the future lines and publications.
- Appendix A briefly introduces genetic algorithms and explains the genetic algorithm used for bandwidth enhancement in Chapter 5.
- Appendix B gathers some Fourier Transform properties, assumed as known in Chapters 3 and 5.

Chapter 2

Phased Array Overview

Contents

2.1 Introduction

A phased array can be defined as a set of antennas, generally identical, whose elements are fed varying their amplitude and phase in order to achieve a more directive pattern. As a general rule, a phased array is studied without considering the mutual coupling between elements. Under that scenario, phased array radiation pattern can be decomposed as the product of two different patterns:

- **Element radiation pattern**: Defined by the antenna type used in the array (e.g. patch, dipole...)
- **Array factor**: It can be considered as the structure radiation pattern. It depends on the number of elements as well as each element excitation and treats each element as an isotropic radiator.

Both patterns are independent from each other, and as a result, are independently studied. Generally, the element radiation pattern is ignored.

General radiation mechanism of a phased array consists of varying the relative phase at each element, so a constructive interference is produced in a certain direction (see section 2.2) and the whole structure becomes more directive, whilst destructive interference is produced in the rest of directions. The constructive interference direction is commonly known as the **scanned** direction (or angle).

The scanned direction is defined by the phase difference between elements. Therefore, a phased array is made not only by the set of antennas but a set of shifters whose role is to phase shift each signal to create the desired constructive interference. A very general scheme of a phased array is shown in Figure 2.1.

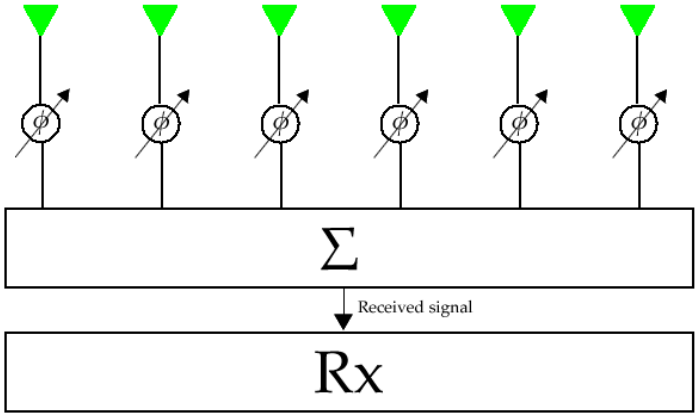

FIGURE 2.1: Phased array block diagram

If this phase difference can be customized in real time, the scanned direction can be modified, so the phased array can be pointing to different directions at different time instants. This property is known as electronic beam steering and constitutes one of the most important properties of phased array antennas since it allows the array to scan over different directions without rotating the array structure [15] and perform it faster than a mechanically rotator antenna would do [16].

The phased array radiation pattern can be derived from different points of view. In this chapter, the two easiest approaches in time and frequency domain will be shown, as they will be later used in this thesis. More sophisticated approaches are: Finite Element Method (FEM) [17], Finite-Difference Time-Domain (FDTD) [18] or the Method of Moments (MoM) [19].

2.2 Phased arrays in time domain

A very easy approach to phased array performance can be done in time domain using plane wave propagation principles. This approach will be expanded in Chapter 5 to

explain the time domain alignment for a generic array.

Assume a linear array over the z axis, whose elements are identical and equally spaced a distance given by d. A plane wave impinges the array with an angle θ_i as shown in Figure 2.2.

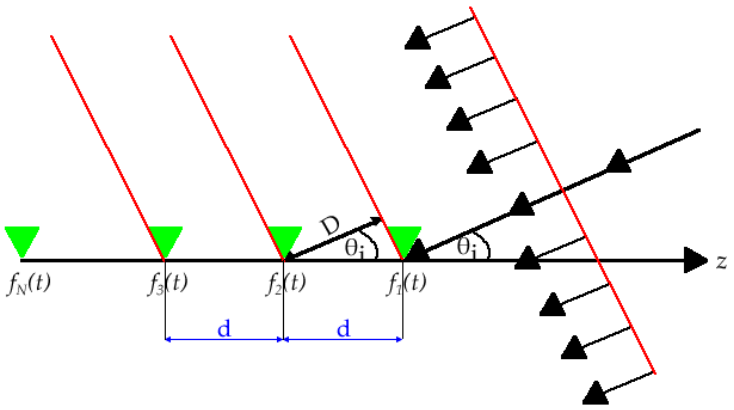

FIGURE 2.2: Linear array incidence in time domain

The phased array problem can be simplified, assuming a linear polarization in the transmitted wave that matches the array elements one. Under this assumption, the electric field received at the n^{th} antenna element, $\vec{E}_n(t)$, generates an electric signal $f_{n,i}(t)$ (the subindex i stands for *incident*). If an ideal scenario is considered (isotropic, non dispersive and homogeneous medium, as well as no Doppler shift and no noise), the signal received at each antenna will be equal but there will be time shifts.

$$f_{n,i}(t) = f_0(t - \Delta_n) \tag{2.1}$$

Where Δ_n stands for the time shift with respect to a time reference (this phase reference will be set to be the signal received at the first antenna, $n = 1$). For the simplified considered case, this time shift can be computed using the plane wave phase front principle. Phase fronts are represented in red in Figure 2.2 and predict the extra space D traveled by a plane wave between the n^{th} and the $n + 1^{th}$ as:

$$D = dcos(\theta_i) \tag{2.2}$$

Assuming free space propagation, the conversion between space and time is direct, so the delay between two consecutive elements is:

$$\Delta t = \frac{dcos(\theta_i)}{c} \tag{2.3}$$

For the sake of simplicity, the first element can be taken as time reference ($f_1, i(t) = f_0(t)$, where $f_0(t)$ stands for the transmitted signal). Given this assumption, the signal received at the n^{th} antenna is:

$$f_{n,i}(t) = f_0\left(t - (n-1)\frac{dcos\left(\theta_i\right)}{c}\right) \tag{2.4}$$

It is possible to align the signals as:

$$f_n(t) = f_{n,i}\left(t + (n-1)\frac{dcos\left(\theta_0\right)}{c}\right) \tag{2.5}$$

An angle θ_0 has been assumed. This angle does not necessarily have to be equal to θ_i since there can be scanning errors. By combining (2.4) and (2.5):

$$f_n(t) = f_0\left(t - (n-1)\frac{d\left(cos\left(\theta_i\right) - cos\left(\theta_0\right)\right)}{c}\right) \tag{2.6}$$

Finally, all the received signals should be added in order to complete the phased array:

$$f(t) = \sum_{n=1}^{N} f_n(t) \tag{2.7}$$

In other words

$$f(t) = \sum_{n=1}^{N} f_0\left(t - (n-1)\frac{d\left(cos\left(\theta_i\right) - cos\left(\theta_0\right)\right)}{c}\right) \tag{2.8}$$

If $\theta_i = \theta_0$ then $f_n(t) = f_0(t)$ for all n. As a result, for a $\lambda/2$ spaced array (like the one that will be considered in Chapter 5) a constructive interference is produced and

$$f(t) = Nf_0(t) \tag{2.9}$$

This result is highly desired, as it allows the phased array to present a processing gain. When $\theta_i \neq \theta_0$ a loss is produced. This loss is difficult to characterize in the time domain, but it is relatively easy to compute in the frequency domain approach using the **array factor**.

2.3 Phased arrays in frequency domain

A more rigorous approach can be done in frequency domain, by considering the received electric fields at the different antenna locations. Let an array made by N antennas. The total received electric field in the phased array, $\vec{E}_{tot}$, can be derived as the sum of each individual received fields, $\vec{E}_n\left(\vec{r}_n'\right)$, as:

$$\vec{E}_{tot} = \sum_{n=1}^{N} \vec{E}_n\left(\vec{r}_n'\right) \tag{2.10}$$

The different antennas will be generally placed in arbitrary positions defined by $\vec{r}_n'$. It is helpful to refer the electric field as if the antennas were located at the origin as:

$$\vec{E}_{tot} = \sum_{n=1}^{N} \vec{E}_{0,n} e^{jk\vec{r}_n'\cdot\hat{r}} \tag{2.11}$$

where $\vec{E}_{0,n}$ stands for the received electric field at the origin and $\hat{r}$ for the unit direction vector (in spherical coordinates) of the incoming plane wave as:

$$\hat{r} = -sin\theta_i cos\varphi_i\hat{x} - sin\theta_i sin\varphi_i\hat{y} - cos\theta_i\hat{z} \tag{2.12}$$

If the array is composed of equal elements and mutual coupling between elements is not considered, the term $\vec{E}_0$ can be normalized as:

$$\vec{E}_{0,n} = A_n\vec{E}_{\tilde{0}} \tag{2.13}$$

Equation (2.13) can be inserted in (2.11):

$$\vec{E}_{tot} = \vec{E}_{\tilde{0}} \sum_{n=1}^{N} A_n e^{jk\vec{r}_n'\cdot\hat{r}} \tag{2.14}$$

The received field $\vec{E}_{0,n}$ is normalized to $\vec{E}_{\tilde{0}}$ and the term A_n is added to indicate the amplitude and phase difference between each antenna excitation. The excitation coefficients can be split into amplitude and phase as:

$$A_n = a_n e^{j\alpha_n} \tag{2.15}$$

By substituting (2.15) in (2.14):

$$\vec{E}_{tot} = \vec{E}_{\tilde{0}} \sum_{n=1}^{N} a_n e^{j\left(k\vec{r}_n' \cdot \hat{r} + \alpha_n\right)} \tag{2.16}$$

Two different terms can be defined in (2.16):

- The $\vec{E}_{\tilde{0}}$ term which is related to the element radiation pattern.
- The summation term, which is generally known as the array factor:

$$AF = \sum_{n=1}^{N} a_n e^{j\left(k\vec{r}_n' \cdot \hat{r} + \alpha_n\right)} \tag{2.17}$$

Equation (2.17) shows the array factor for the most generic case. If all the elements in the array are equally spaced d and placed over the z axis, then:

$$\vec{r}_n' \cdot \hat{r} = -(n-1)dcos(\theta_i) \tag{2.18}$$

Hence, (2.17) becomes:

$$AF = \sum_{n=1}^{N} a_n e^{j(-k(n-1)dcos(\theta_i) + \alpha_n)} \tag{2.19}$$

It is common to set all the antennas excitation amplitude equal to 1 and a progressive phase shift between elements. This feeding allows the array to be scanned at a direction θ_0 by setting the progressive phase α_n as:

$$\alpha_n = (n-1)\, kdcos(\theta_0) \tag{2.20}$$

Equation (2.20) can be inserted into (2.19) obtaining:

$$AF = \sum_{n=1}^{N} e^{jk(n-1)d(cos(\theta_0) - cos(\theta_i))} \tag{2.21}$$

The variable ψ is commonly used to avoid angle references in the array factor:

$$\psi = kd\,(cos(\theta_0) - cos(\theta_i)) \tag{2.22}$$

Equation (2.21) is often written in the following fashion:

$$AF = e^{j(N-1)\frac{\psi}{2}} \frac{sin\left(\frac{N\psi}{2}\right)}{sin\left(\frac{\psi}{2}\right)} \tag{2.23}$$

Equations (2.21) and (2.23) presents their maximum at $\psi = 2m\pi$ with m integer. If the array elements are spaced not further than half a wavelength apart, the only possible value for m is 0, so the array factor is maximum when $\theta_i = \theta_0$, in other words, a constructive interference is produced if the scanned and the incoming angle are equal. For those cases where it is possible to obtain $|\psi| > 2\pi$ grating lobes are produced, that is, it is possible to create a constructive interference in more than one direction, hence the array factor becomes multilobed (which is not generally a desired situation).

These results (specially (2.21)) will appear throughout the thesis, and will be used to prove that the novel technique proposed in Chapter 3 and expanded in Chapter 5 is equivalent in terms of radiation pattern to the traditional phased array approach explained here.

2.4 Beamforming techniques

As introduced in Chapter 1, beamforming is a technique to perform spatial filtering which generates a more directive radiation pattern by combining signals originated at different space locations [20]. Given N equal antennas, the total radiation pattern can be adjusted by modifying the relative weight of each antenna element and, more important, the relative delay between elements. An appropriate delay yields to time domain aligned signals.

Although the ideal beamforming is performed using true-time delay, this approach is not often used due to its complexity. Hence, signal alignment is generally performed using phase shifting. It has been introduced in Chapter 1 that beamforming can be performed either in analog domain [21], or digital domain [22, 23]. A third option is the hybrid domain, which is a combination of both two [24, 25].

2.4.1 Analog Beamforming

Beamforming in analog domain is performed before signals are sampled. In other words, the spatial filtering is done before the received signals are digitized. There are

many architectures that can carry out analog beamforming, depending on the stage where phase shifting is performed [26].

- RF Beamforming: The most intuitive and most used one [27]. The phase shift is directly applied to the received signal in RF before downconverting to IF. The theoretical derivations made in this chapter assume RF beamforming.
- IF Beamforming: It is the dual to RF beamforming. The signal is first downconverted to IF and then phase shifted [28].
- LO Beamforming: It is a combination of previous techniques. Downconverting and phase shifting are simultaneously performed by delaying the local oscillator (LO) [29].

Phase shifting becomes a key step in analog beamforming, so the election of an adequate technique is critical in the system performance. Some classical technologies are listed below [27, 30–33].

- Stripline diode
- Dual mode ferrite
- Toroidal ferrite
- Ferroelectric materials
- Microwave integrated circuits (MMICS)
- Microelectromechanical systems (MEMS)
- Varactor diode

Analog beamformers are intuitive and simple. However, they present an important disadvantage in terms of cost, since phase shifters are expensive and lossy devices. In addition, traditional phased array architectures consider one phase shifter per antenna, increasing the system cost proportionally to the array size.

2.4.2 Digital Beamforming

Another approach is to perform beamforming in digital domain. This way, one can get rid of shifters at the cost of a computationally more expensive system. The idea is to digitize the received signal in I/Q channels and apply a digital phase shift. Digital beamforming can be performed at IF or RF.

- IF Digital Beamforming: The received signal is downconverted and sampled.
- RF Digital Beamforming: The received signal is directly sampled (after the low noise amplifier) and downconverted afterwards.

RF Digital Beamforming seems a more appropiate option, since the sampled signal is the original one. However, as the carrier frequency and the number of elements increase, the sampled data becomes impossible to handle. In addition, RF ADC's generally present a very low resolution. As a result, the sampled signal will show large quantization noise, leading to poor signal to noise ratio.

Chapter 3

Proposed sampling scheme

Contents

3.1 Proposed sampling scheme description

A phased array can be understood as an independent set of antennas in which all elements receive a common information which is the amplitude of the received signal (equal for all elements except for the additive noise), and a unique information provided by the space location that yields to different relative delay between elements. The common information gives redudancy and can be removed to simplify the system. This idea is the key of the proposed scheme, and therefore, of the actual thesis.

The traditional phased array approach consists of sampling simultaneously all the antennas, and afterwards, aligning them using the time/phase difference predicted by the relative position between them. The technique proposed in this thesis also takes in

account the time/phase difference between elements, but only one antenna is sampled during each RF cycle. The relative delay between two antennas located at $\vec{r}_1$ and $\vec{r}_2$ is:

$$\Delta t_{12} = \frac{(\vec{r}_1 - \vec{r}_2) \cdot \hat{r}_i}{c} \tag{3.1}$$

The algorithm for the proposed technique (actually, this algorithm will be later generalized and this particular approach will be named as **minimum delay**) is:

I Select the antenna closest to the source and sample it during one RF cycle.

II Wait until the next RF cycle arrives to the next antenna, which is the second one in terms of distance to the source. This waiting time is the same as the delay predicted by traditional phased array theory.

III Sample the second antenna during a RF cycle.

IV Repeat II and III until reaching the last antenna and return to I.

The proposed technique can be seen in Figure 3.1, where the previous algorithm is represented for a five element array. It can be seen that after aligning all the elements, the resulting signal is the continuous transmitted signal. It is important to outline that the sampling process in this stage is **analog**.

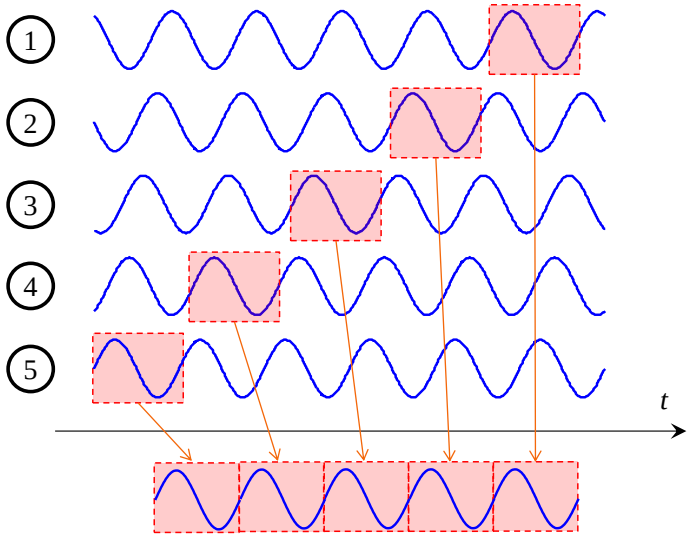

FIGURE 3.1: Proposed sampling scheme

Since the proposed sampling technique only considers the information that is required to reconstruct the signal and does not deal with redundant data, it can be described

as an **economic sampling scheme**. The term *economic sampling* is inspired in a signal processing technique known as *compressed sensing* or *compressive sampling* [34, 35].

Compressed sensing states that it is possible to improve the acquisition process by optimizing it. The traditional acquisition process consist of sampling an information source using a sampling frequency higher than the one predicted by Nyquist theorem. The sampled data is stored in a desired representation system and it can be compressed by discarding the least meaningful coefficients . This process is represented in Figure 3.2.

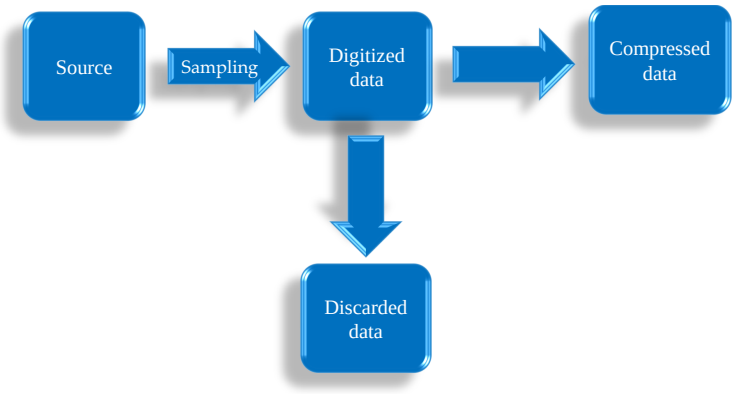

FIGURE 3.2: Traditional acquisition process

Compressed sensing states that there is no point in putting effort into sampling data which is going to be discarded. Hence, only data that will be needed in future should be acquired. This sampling policy is known as economic sampling and is represented in Figure 3.3.

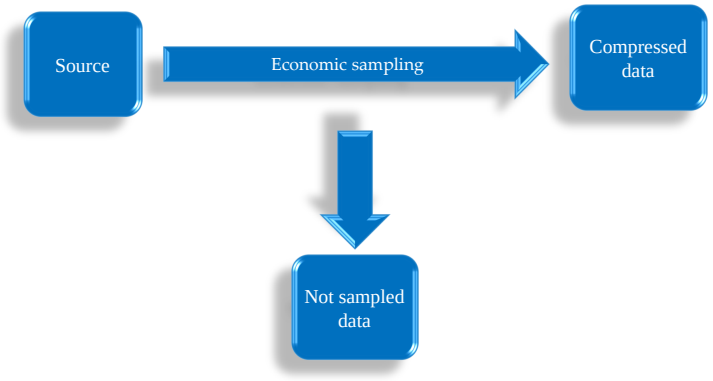

FIGURE 3.3: Economic acquisition process

The discarded data set in Figure 3.2 and the not sampled data set in Figure 3.3 are identical. However, in the second case, the system has never sampled the discarded information, yielding to a more efficient process.

Compressed sensing is an estimation problem. In other words, the final signal will be obtained using a minimizing error technique and works better for sparse signals (those signals that can actually be recovered using a sampling frequency lower than the predicted by Nyquist theorem). On the other hand, the technique proposed in this thesis only samples information that will be later used avoiding redundancies (the amplitude information at each antenna) but it does not perform any kind of estimation process. As a result, it cannot be considered as a compressed sensing problem, but it is based on the same economic sampling principles.

3.2 Mathematical derivation

The proposed technique can be mathematically proved for a linear array. Assume a N element linear array, whose elements are equally spaced $\lambda/2$ and placed along the z axis. A plane wave impinges this array with an angle θ_i. In order to provide mathematical evidence of the proposed technique, an analytic model of the array as well as the sampling and switching process must be provided. This model is illustrated in Figure 3.4, where the array layout and the switching signals are depicted. The resulting signal is equivalent to that represented in 3.1. The wait time introduced in Figure 3.1 is represented as $\frac{dcos\theta_0}{c}$, which is the predicted propagation delay between two consecutive antennas.

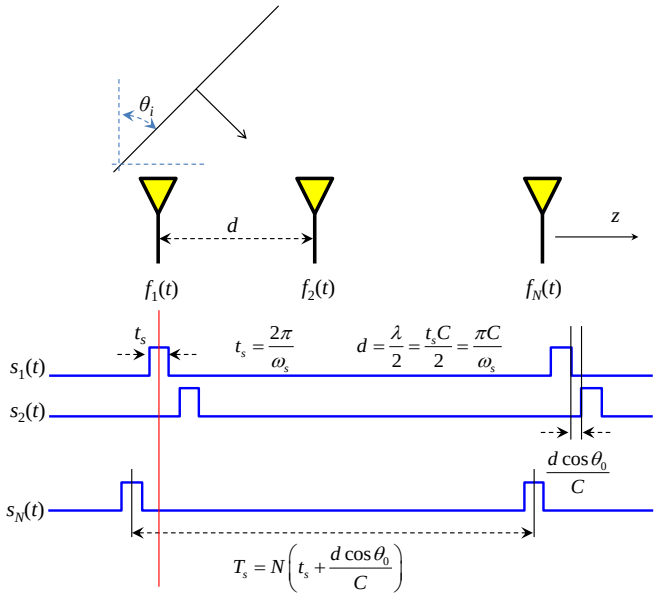

FIGURE 3.4: Array layout and resulting switching scheme

Let $f_0(t)$ be the transmitted signal, and $f_n(t)$ the received signal at the n^{th} antenna. Without loss of generality, let the first antenna be the time reference. The received signal at each antenna can be written as:

$$f_n(t) = f_0\left(t - (n-1)\frac{dcos(\theta_i)}{c}\right) \tag{3.2}$$

Note that, according to (3.2)

$$f_1(t) = f_0(t) \tag{3.3}$$

This result does not take in account the propagation time between the transmitter and the first antenna, hence, at first glance it can be considered as not rigorous. However, the propagation time can be dropped, since it is common to all the antennas and does not affect to the final result leading to an easier mathematical derivation.

The sampling process can be modeled as a sum of the incident signals windowed by a set of switching signals. The switching signals are represented by $s_n(t)$, where n stands for the n^{th} antenna. Since the process must be continuous (in other words, after sampling the last antenna, we should come back to the first and repeat the whole process again) the switching signals must be periodic with period T_s. The general form of the switching signal (without characterizing for the n^{th} antenna) is :

$$s(t) = \sum_{m=-\infty}^{\infty} \Pi\left(\frac{t - mT_s}{t_s}\right) \tag{3.4}$$

where t_s stands for the sampling time window (the time lapse that each individual antenna is sampled). Since the idea is to sample each antenna during a RF cycle, t_s is the cycle period of the RF carrier. The function $\Pi(t)$ refers to a rectangular pulse centered at the origin and unit width.

$$\Pi(t) = \begin{cases} 1 & |t| < \frac{1}{2} \\ 0 & elsewhere \end{cases} \tag{3.5}$$

According to the switching scheme shown in Figure 3.4, the aperture sampling period T_s (time lapse between two sampling processes in the same antenna) is:

$$T_s = N\left(ts + \frac{dcos\,(\theta_0)}{c}\right) \tag{3.6}$$

In other words, the aperture sampling period is obtained as the summation of the N sampled cycles and the waiting times. For a $\lambda/2$ spacing, the sampling aperture period is:

$$T_s = N t_s \left(1 + \frac{cos\left(\theta_0\right)}{2}\right) \tag{3.7}$$

where θ_0 stands for the array scanned angle. Note that scanned angle and received angle do not need to necessarily match, although it is highly desirable in order to have higher gain (and undesirable in the case of an interfering signal). An aperture sampling rate can be defined as:

$$\Omega_s = \frac{2\pi}{T_s} \tag{3.8}$$

In order to take account of the relative delay between elements, each $s_n(t)$ should be delayed as:

$$s_n\left(t\right) = s\left(t - \left(n-1\right)\left(t_s + \frac{d\cos\theta_0}{c}\right)\right) \tag{3.9}$$

It is interesting to compare the delay experienced by the received signal in (3.2) and the delay applied to the switching signal in (3.9). Only if $\theta_i = \theta_0$ received and switching signals are in phase.

Equation (3.9) can be rewritten in a more convenient way by applying $d = \frac{\lambda}{2}$ as:

$$s_n\left(t\right) = s\left(t - t_s\left(n-1\right)\left(1 + \frac{\cos\theta_0}{2}\right)\right) \tag{3.10}$$

Given the received signal at (3.2) and the switching signal at (3.10), the final step is to align the different cycles (e.g. using a synchronized switch) and remove the time gaps between antennas. This process can be modeled as:

$$f\left(t\right) = \sum_{n=1}^{N}\left(f_n\left(t\right)s_n\left(t\right)\right) * \delta\left(t - \left(N-n\right)\frac{d\cos\theta_0}{c}\right) \tag{3.11}$$

Where $\delta(t)$ stands for the Dirac delta. It is easier to study this equation in the frequency domain. The Fourier Transform of (3.11) is (refer to Appendix B):

$$F(\omega) = \frac{1}{2\pi} \sum_{n=1}^{N} \left(F_n(\omega) * S_n(\omega) \right) e^{-j\omega(N-n)\frac{d\cos\theta_0}{C}} \tag{3.12}$$

The term $S_n(\omega)$ can be obtained by computing the Fourier Transform of (3.10) as:

$$S_n(\omega) = \frac{2\pi t_s}{T_s} \sum_{m=-\infty}^{\infty} e^{-j\frac{2\pi\, m(n-1)}{N}} sinc\left(\frac{m\pi t_s}{T_s}\right) \delta\left(\omega - \frac{2m\pi}{T_s}\right) \tag{3.13}$$

After substituting (3.13) in (3.12) and applying the convolution:

$$F(\omega) = \frac{t_s}{T_s} \sum_{n=1}^{N} e^{-j\omega(N-n)\frac{\pi\cos\theta_0}{\omega_s}} \sum_{m=-\infty}^{\infty} e^{-j\frac{2\pi\, m(n-1)}{N}} sinc\left(\frac{m\pi t_s}{T_s}\right) F_n(\omega - m\Omega_s) \tag{3.14}$$

$F_n(\omega)$ can be easily derived as the Fourier Transform of (3.11)

$$F_n(\omega) = F_0(\omega)\, e^{-j\omega(n-1)\frac{\pi\cos\theta_i}{\omega_s}} \tag{3.15}$$

By substituting (3.15) in (3.14):

$$\begin{aligned} F(\omega) = \tfrac{t_s}{T_s} \sum_{n=1}^{N} e^{-j\omega(N-n)\frac{\pi\cos\theta_0}{\omega_s}} \sum_{m=-\infty}^{\infty} e^{-j\frac{2\pi\, m(n-1)}{N}} \\ \cdot sinc\left(\tfrac{m\pi t_s}{T_s}\right) F_0(\omega - m\,\Omega_s)\, e^{-j(n-1)(\omega - m\,\Omega_s)\frac{\pi\cos\theta_i}{\omega_s}} \end{aligned} \tag{3.16}$$

Equation (3.16) can be easily interpreted by swapping the summation order and rearrange the exponential terms as:

$$\begin{aligned} F(\omega) = \tfrac{t_s}{T_s} e^{-j\pi(N-1)\frac{\omega\cos\theta_0}{\omega_s}} \sum_{m=-\infty}^{\infty} sinc\left(\tfrac{m\pi t_s}{T_s}\right) \\ \cdot F_0(\omega - m\,\Omega_s) \sum_{n=1}^{N} e^{-j\pi(n-1)\left\{\frac{\omega}{\omega_s}(\cos\theta_i - \cos\theta_0) + \frac{mt_s}{T_s}(2 + \cos\theta_0 - \cos\theta_i)\right\}} \end{aligned} \tag{3.17}$$

Equation (3.17) shows a very representative result of the received signal. This received signal is composed of an infinite series of harmonics, spaced Ω_s, weighted by a sinc function and an additional term. It is possible to filter around the main harmonic, $m = 0$, to avoid undesired frequency components obtaining:

$$F_{filtered}(\omega) = \frac{t_s}{T_s} e^{-j\pi(N-1)\frac{\omega\cos\theta_0}{\omega_s}} F_0(\omega) \sum_{n=1}^{N} e^{-j\pi(n-1)\frac{\omega}{\omega_s}(\cos\theta_i - \cos\theta_0)} \tag{3.18}$$

The summation term in (3.18) is equivalent to:

$$\sum_{n=1}^{N} e^{j(n-1)\beta d(\cos\theta_0 - \cos\theta_i)} \tag{3.19}$$

Which is the array factor for a uniform linear array (2.21) [36] scanned to θ_0 which is receiving a signal from angle θ_i. This result shows an equivalence between the proposed technique and the traditional phased array approach. Figure 3.5 shows a radiation pattern comparison between the traditional phased array and the proposed technique. The comparison is illustrated by plotting the radiation pattern for a 16 element linear array scanned to $\theta_0 = 0°$ and $\theta_0 = 30°$ using both methods. The radiation patterns are identical to each other.

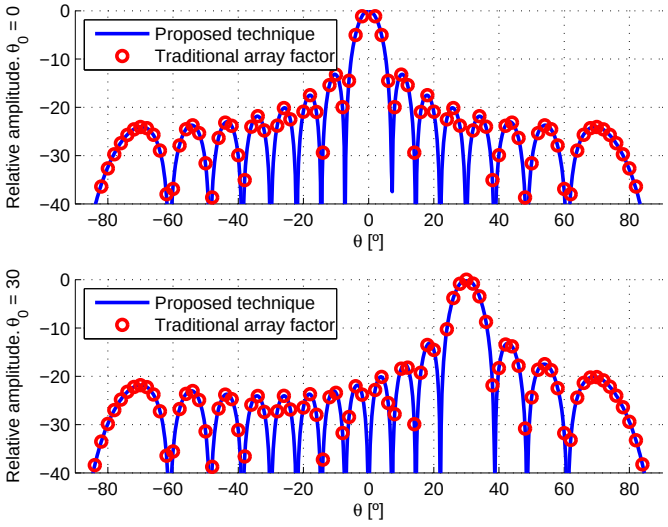

FIGURE 3.5: Radiation pattern for a 16 element linear array scanned to $\theta_0 = 0$ and $\theta_0 = 30$ obtained using the traditional array factor and the proposed technique

3.3 Block Diagram

According to the derivation in Section 3.2, the proposed phased array receiver is composed of:

- Receiver front-end: Made of N antenna/LNA combinations.
- Switch: Receiver core. Analogically samples the antennas.
- Anti-aliasing filter: Rejects the undesired harmonics ($m \neq 0$).

A basic phased array receiver based on the proposed technique is completed by adding an ADC an a processing unit, as shown in Figure 3.6.

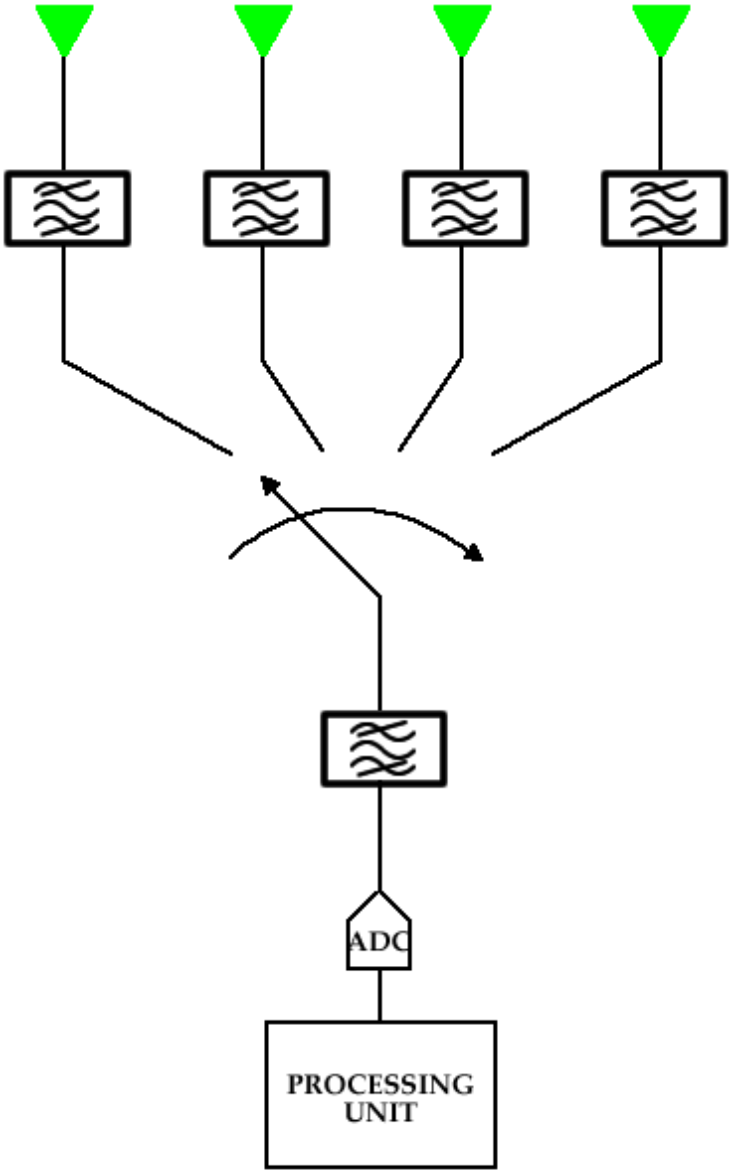

FIGURE 3.6: Proposed technique block diagram using RF analog to digital conversion

This first approach is very intuitive, since it is a direct representation of the mathematical derivation in Section 3.2. However, it might not be very practical, because of the analog to digital conversion performed in RF, as these devices generally present low resolution and thus, poor signal to noise ratio. A possible solution is to down-convert the sampled signal to IF and after that, perform analog to digital conversion, as shown in Figure 3.7. It should be mentioned that the block diagrams in Figures 3.6 and 3.7 are not the only possible solution and that the optimum architecture will depend

on the transmitted signal frequency, as well as the system requirements. Other possible approaches are individual down-converting before analog sampling or double IF down-converting.

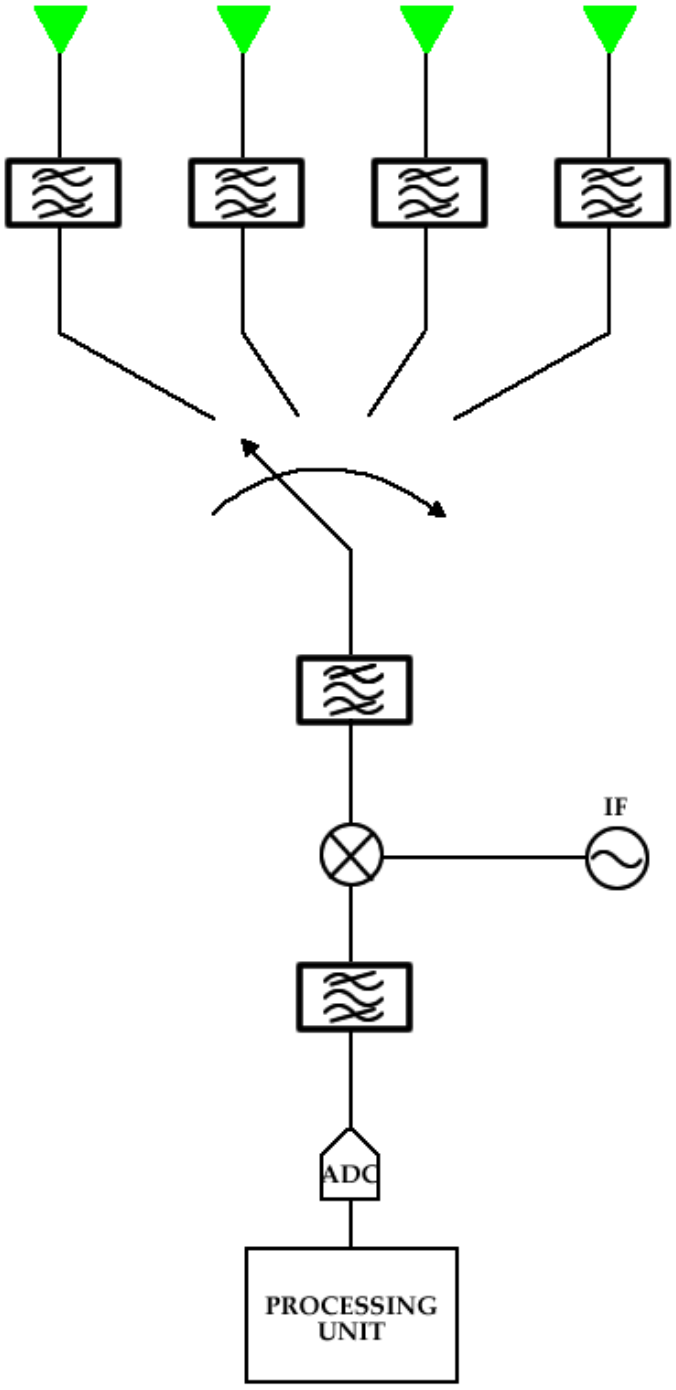

FIGURE 3.7: Proposed technique block diagram using IF analog to digital conversion

3.4 Bandwidth limit

According to (3.17), the summation of different harmonics yields a limitation in the signal bandwidth in a similar way as Nyquist theorem does. Equation (3.17) can be rewritten in a more convenient way as:

$$F(\omega) = A \sum_{m=-\infty}^{\infty} F_0(\omega - m\Omega_s)\Lambda(\omega, \theta_i, \theta_0, m, \omega_S, t_s) \tag{3.20}$$

where A is a constant that does not affect the radiation pattern and the term Λ shows that a distortion is produced in all the harmonics but the principal one. For $m = 0$ and $\theta_i = \theta_0$ it is obtained that $\Lambda = 0$, hence:

$$F(\omega) = NAF_0(\omega) \tag{3.21}$$

As a result, transmitted and received signals are likely to be identical. However, this statement is not always true. Equations (3.17) and (3.20) suggest that if the signal is wideband, the first harmonic may overlap with the main one causing aliasing. A representation of the received signal for the main and the first harmonic is depicted in Figure 3.8

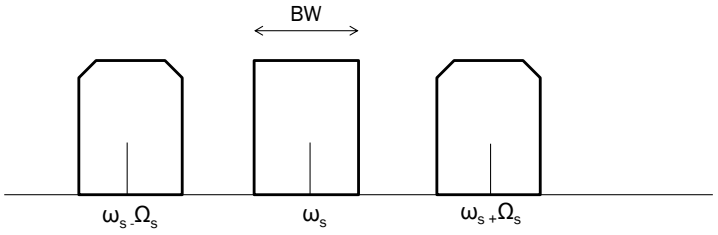

FIGURE 3.8: Main and first harmonic representation

In order to avoid aliasing, the highest frequency component of the main harmonic must be smaller than the lowest frequency component of the first harmonic. Mathematically:

$$\omega_s + \frac{BW}{2} = \omega_s + \Omega_s - \frac{BW}{2} \tag{3.22}$$

The condition to avoid aliasing is:

$$\Omega_s > BW \tag{3.23}$$

which is the aperture Nyquist limit. The worst case scenario is produced for $\theta_0 = 0$ (endfire situation, which yields larger waiting time and as a result, larger aperture sampling period), when the aperture sampling period is maximum and equal to:

$$T_{s,max} = \frac{3Nt_s}{2} \tag{3.24}$$

Equation (3.23) combined with (3.24) imposes a maximum number of elements as:

$$N \leq \frac{2\omega_s}{3BW} \tag{3.25}$$

So, the maximum number of elements in the array is given by the ratio carrier frequency / signal bandwidth. In other words, the system bandwidth is very narrow for large arrays.

3.5 Linear array simulation

Once the proposed method has been introduced and mathematically proved, it is convenient to validate its performance by simulation. The linear array simulation results include a study of the received signal in both time domain and frequency domain, as well as the radiation pattern (compared to that obtained using the traditional phased array approach).

3.5.1 Received signal

As previously commented, the proposed technique performs some kind of TDMA by sampling each antenna during a RF cycle taking into account the relative delay between elements. According to (3.17) If the array scanned angle and the incoming angle are identical, the received signal will correctly align, giving as a result a continuous signal. In the case they are not identical, the angle mismatch will cause some amplitude hops in the time domain, that will translate into harmonic presence in the frequency domain.

As in the mathematical derivation. assume a 16 element linear array, whose elements are equally spaced $\lambda/2$ but over the x axis. This array receives a pure monochromatic signal at $f = 1$ GHz with an incoming angle $\theta_i = 30$.

In order to show the system performance, Figure 3.9 shows the received signal in the time domain when the array is scanned to $\theta_0 = \{0, 30, 60, 90\}$. It can be easily seen that

only for $\theta_i = \theta_0$ is the received signal a pure tone. For the other three cases, the signal discontinuities will cause the appearance of frequency components as shown in Figure 3.10

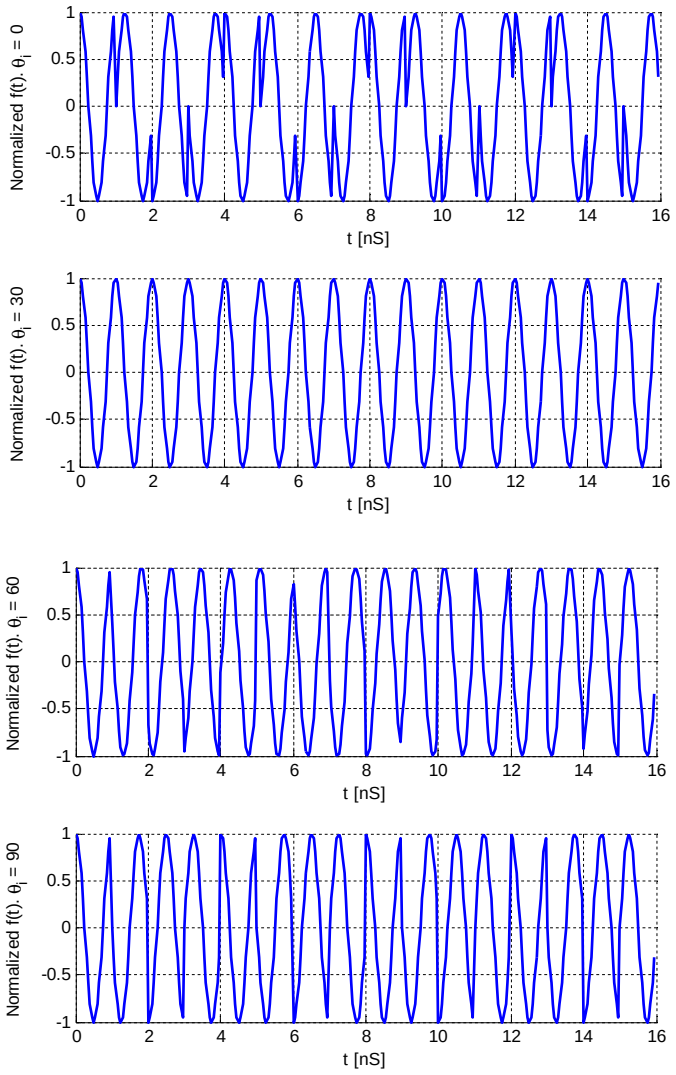

FIGURE 3.9: Received signal in time domain for a 16 element array scanned to 4 different angles

The proposed technique converts an angle mismatch into a frequency shift. This statement is illustrated by Figure 3.10. The original transmitted 1 GHz tone only remains for the case $\theta_i = \theta_0$. Hence, it is possible to filter the signal to reject the components created when $\theta_i \neq \theta_0$. The sampling+filtering process will allow the system to perform beamforming.

The final step in the receiving process consists of filtering. For the current simulation, a 200 MHz Butterworth fifth order filter has been applied to the received signal. The

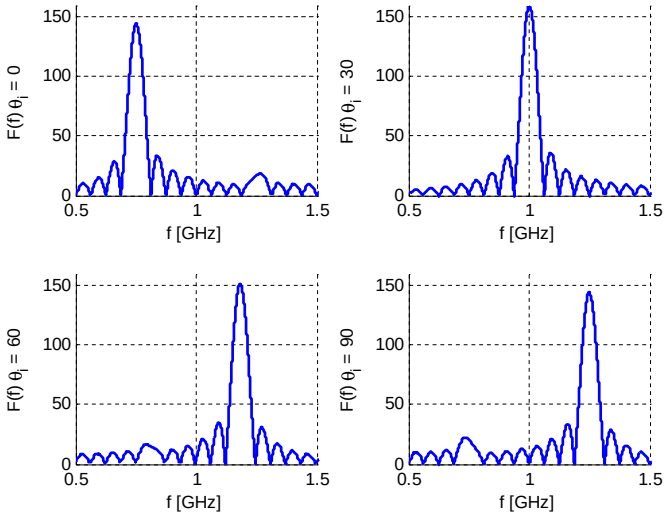

FIGURE 3.10: Received signal in frequency domain for a 16 element array scanned to 4 different angles

results are shown in Figure 3.11. After an initial transient state the signal gets stable with unit values for $\theta_i = \theta_0$ and negligible (but not zero because of the secondary lobes) when $\theta_i \neq \theta_0$. This result is equivalent to the traditional reception problem using any antenna.

3.5.2 Radiation pattern

According to (3.18), the received signal can be written as a function of the traditional array factor shown in (3.19). Since the array radiation pattern is given by the array factor, the proposed technique radiation pattern must be identical to that obtained using the traditional phased array approach. This statement will be checked in this section.

Figure 3.12 shows the radiation pattern for a 32 element $\lambda/2$ spaced linear array. The radiation pattern is represented for 3 different scanned angles ($\theta_0 = \{0, 30, 90\}$) in the principal cut $\varphi = 90$. The array elements are located over the x axis. The traditional phased array approach and the proposed technique approach are exactly identical for the three curves. The radiation pattern is computed by simulating the reception of a pure tone and taking the amplitude of the Fourier Transform at the transmitted frequency.

A well-known result in phased array theory is the relation between the array size and the radiation pattern beamwidth. A higher number of elements yields a more directive radiation pattern. This statement can also be seen from an aperture viewpoint: the higher the aperture area, the higher the gain.

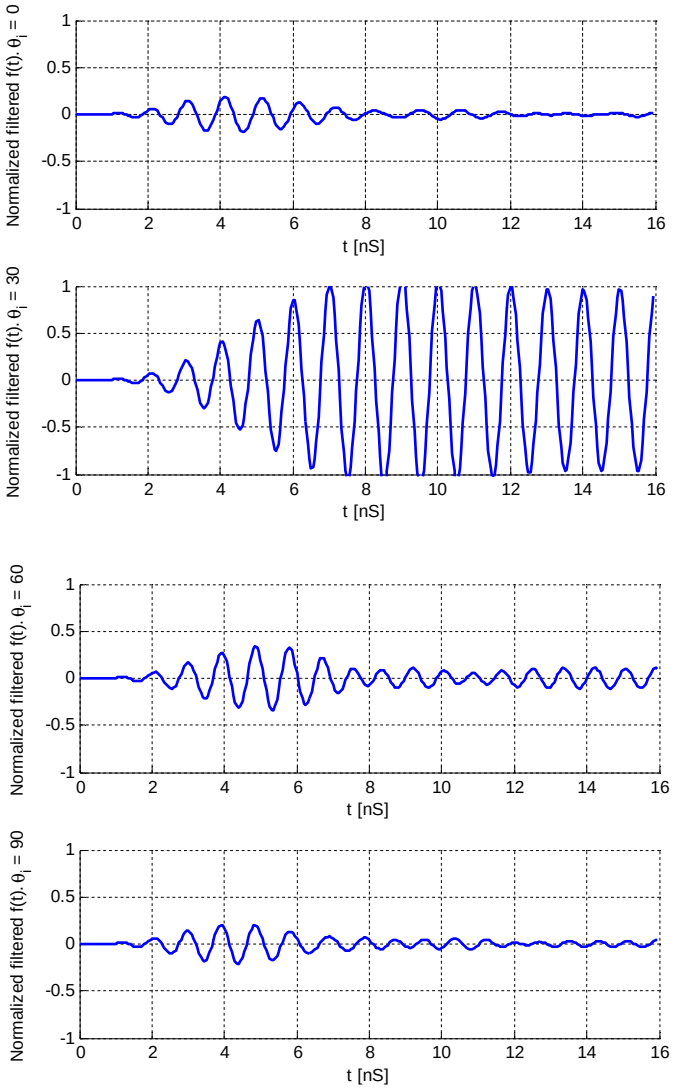

FIGURE 3.11: Received signal in time domain for a 16 element array scanned to 4 different angles after applying a 200 MHz Butterworth fifth order filter

Figure 3.13 illustrates the radiation pattern dependence on the array number of elements. A broadside array radiation pattern is represented as a function of the number of antennas in it, from 4 to 64. As was expected, the beamwidth reduces as the number of elements increases. It also should be mentioned that these curves are equivalent to those obtained using the traditional phased array approach.

Figures 3.12 and 3.13 show the radiation pattern in a principal cut. It is interesting to show the radiation pattern in 3D to obtain a better view of it. Figures 3.14, 3.15 and 3.16 show the 3D representation for three different arrays placed over the x axis, combining different number of elements and scanned directions. Figure 3.14 represents

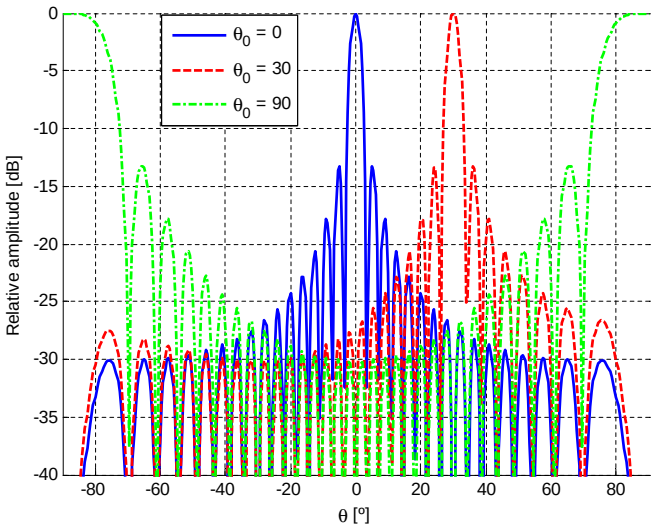

FIGURE 3.12: 32 element linear array radiation pattern for $\theta_0 = \{0, 30, 90\}$ in the principal cut $\varphi = 90$

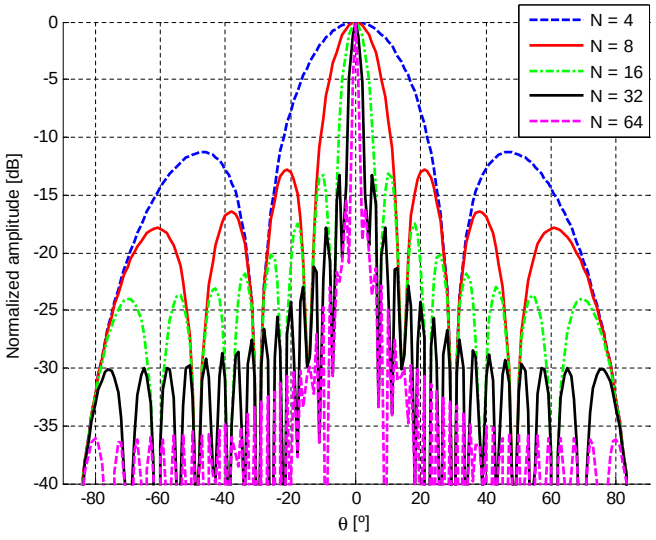

FIGURE 3.13: Broadside linear array radiation pattern for $N = \{4, 8, 16, 32, 64\}$

an 8 element broadside array, Figure 3.15 shows a 16 element linear array scanned to $\theta_0 = 30$ and Figure 3.16 depicts a 64 element endfire array.

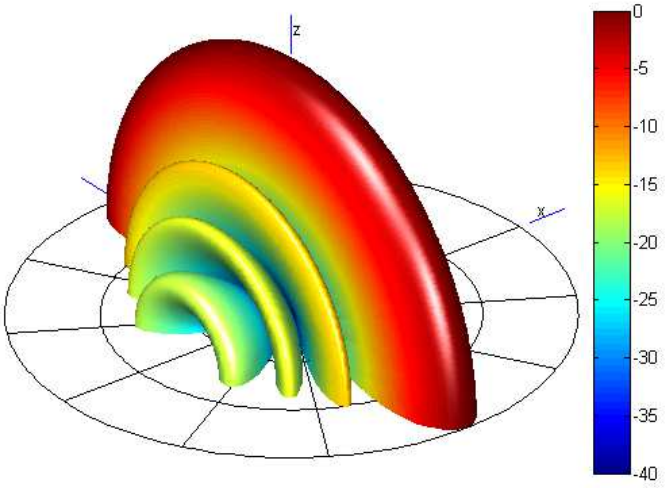

FIGURE 3.14: 8 element broadside array 3D radiation pattern

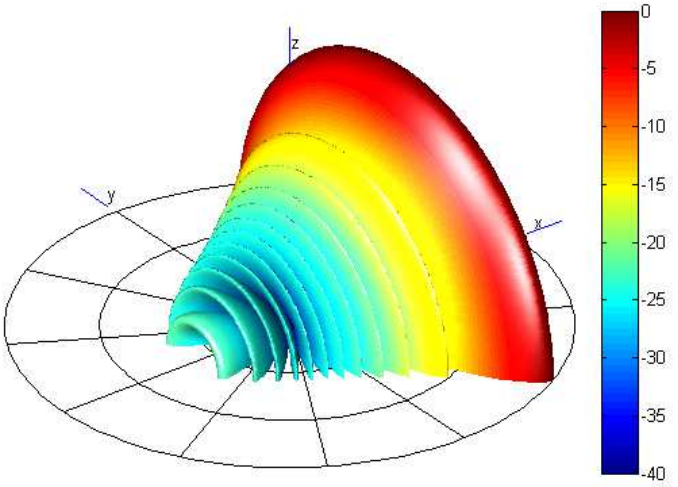

FIGURE 3.15: 16 element array scanned to $\theta_0 = 30$ 3D radiation pattern

As a consequence of the linear array symmetry, all radiation patterns must present a symmetry revolution, in this case around x axis. As a result, it is not possible to design a pencil beam radiation pattern using a linear element distribution. This inconvenient can be overcome by using planar arrays.

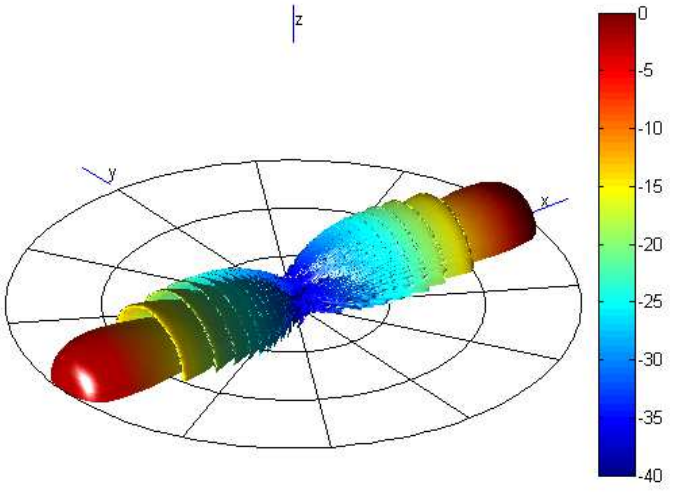

FIGURE 3.16: 64 element endfire array 3D radiation pattern

3.6 Planar array simulation

Planar arrays break with the linear array revolution symmetry, yielding to the possibility of obtaining a pencil beam radiation pattern scanned to (θ_0, φ_0). The previous section study is repeated below to check planar array performance.

Assume a 64 element planar array, organized in an 8×8 grid over the plane $z = 0$, whose elements are equally spaced $\lambda/2$ in both, x and y dimension. This array can be scanned to any (θ_0, φ_0) desired direction. Figure 3.17 shows the radiation pattern for the case $(\theta_0, \varphi_0) = (30, 0)$. A plane wave impinges this array from four different directions: $(\theta_i, \varphi_i) = (0, 0)$, $(\theta_i, \varphi_i) = (30, 0)$, $(\theta_i, \varphi_i) = (60, 0)$ and $(\theta_i, \varphi_i) = (90, 0)$.

The spectral resolution in Figure (3.18) is more accurate than in Figure (3.10) because of the number of considered cycles (16 against 64). Although the angle mismatch is the same in both figures, the frequency shift is smaller in Figure (3.10) because of the higher number of elements which enforces a slower sampling rate. As a consequence, the filter process gets more complicated and only narrowband signals can be transmitted. A 40 MHz fifth order Butterworth filter is applied to reject the undesired components (note that the maximum baseband bandwidth is 20 MHz). The time domain resulting signal is shown in Figure 3.19. Conclusions from Figure 3.19 are similar to those commented in Figure 3.11. An angle mismatch causes an amplitude reduction, not as severe in this case because of the difficulty of rejecting the secondary harmonics due to their close location to main harmonic. Another interesting point is the longer transient time caused by the filter narrower passing band.

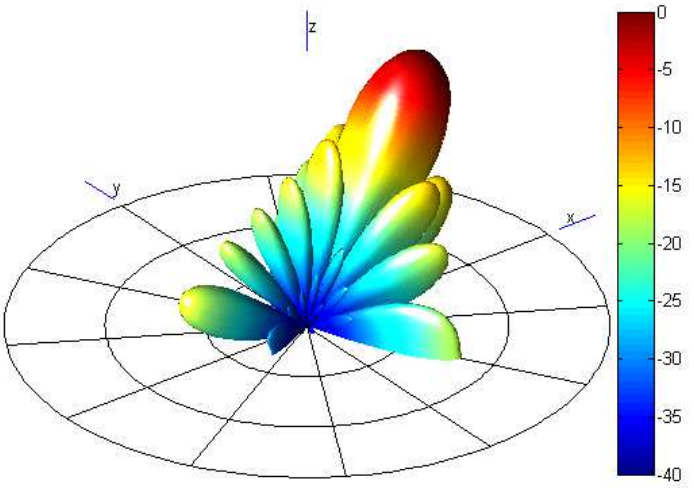

FIGURE 3.17: 8×8 array scanned to $(\theta_0, \varphi_0) = (30, 0)$ 3D radiation pattern

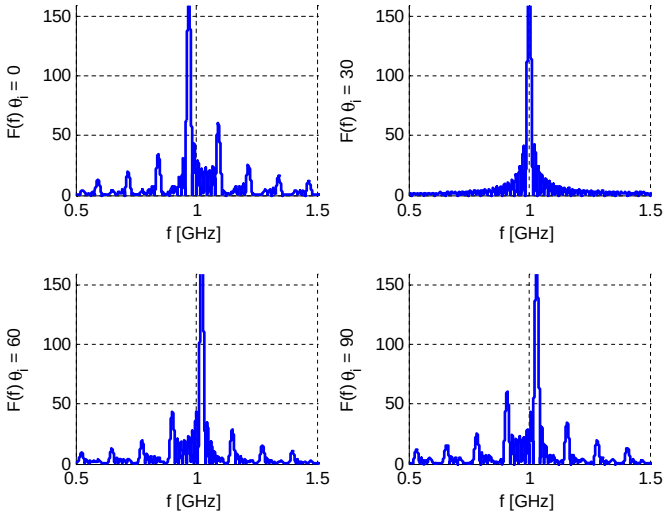

FIGURE 3.18: Received signal in frequency domain for a 64 element planar array as a function of the incoming angle

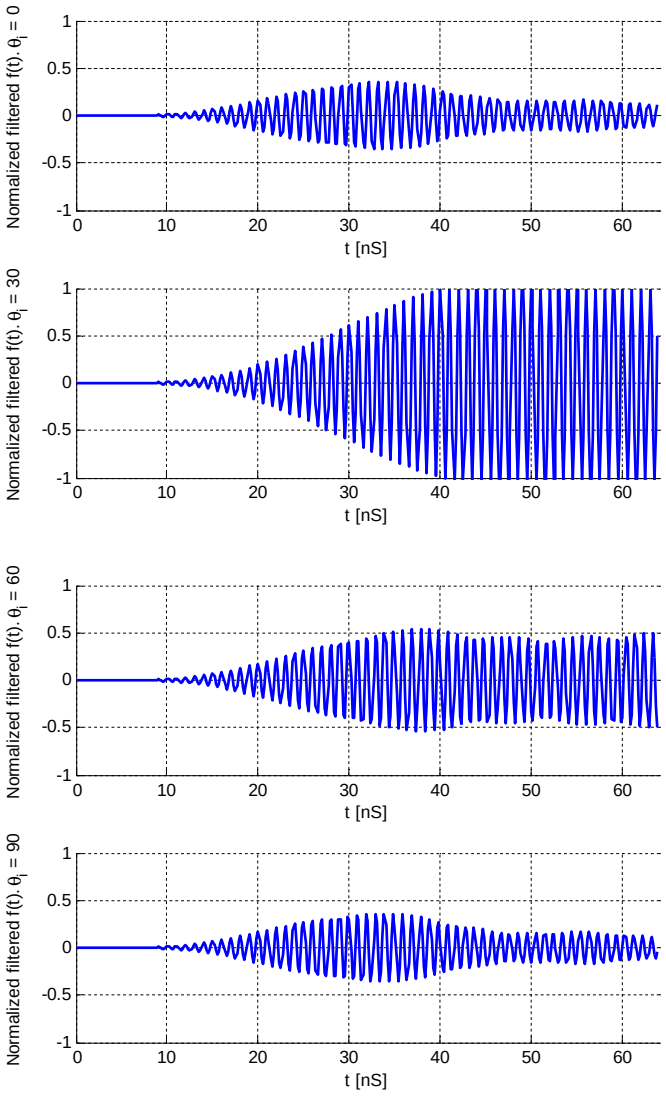

FIGURE 3.19: Received signal in time domain for a 64 element planar array as a function of the incoming angle after applying a 40 MHz fifth order Butterworth filter

3.7 Bandwidth performance

So far, the proposed method has been proved for linear and planar arrays under the assumption of monochromatic waves. This assumption, useful to perform mathematical derivations, is not practical since a transmitted signal must contain bandwidth to carry information. In this section, a DSB (double side band) signal is transmitted, using as a modulating signal a 50 MHz pure tone. An example of received signal is shown in Figure 3.20. The received signal is represented for one cycle of the modulating tone. The array number of elements is set to four, which can be concluded by observing the signal amplitude as there are four RF cycles between silent times. When dealing with

bandwidth transmission it is critical to manage correctly the silent time. In this chapter, the silent time (T_{si}) has been computed using the timing at 3.4 as:

$$T_{si} = T_s - Nt_s = Nt_s \frac{cos(\theta_0)}{2} \tag{3.26}$$

Since the array elements are equally spaced, (3.26) can be easily explained. The silent time is the difference between the aperture sampling period and the total RF sampled period, which is the number of antennas times the RF cycle period. In Chapter 5, the sampling scheme will be generalized to an arbitrary element distribution.

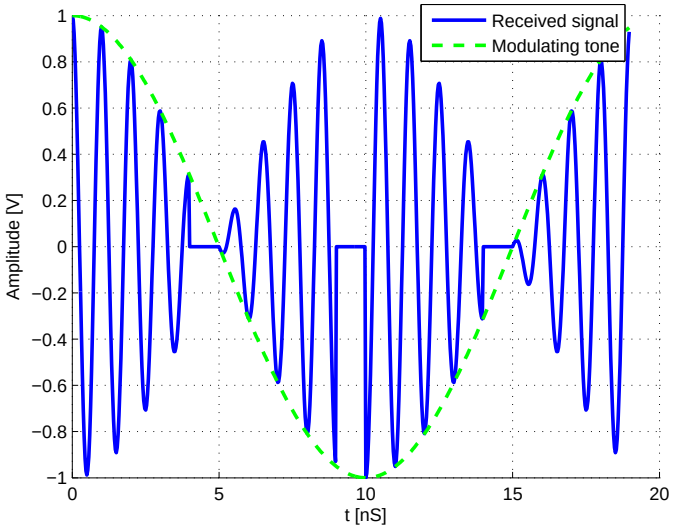

FIGURE 3.20: Example of a received DSB signal. The modulating signal is a 50 MHz pure tone and the carrier frequency is 1 GHz.

3.7.1 Bandwidth signal simulation

Assume a four element linear array, half a wavelength spaced, scanned to $\theta_0 = 30$. This array receives a DSB signal as the one described in Figure 3.20 (the modulating signal is a 25 MHz pure tone and the carrier frequency is 1 GHz) during 80 RF cycles. The wave impinges on the array with three different angles: $\theta_i = 30$, (angle coincidence) $\theta_i = 36$ (small scanning error) and $\theta_i = 60$ (large scanning error, which can be a sign of an interfering signal).

Figure 3.21 shows the Fourier Transform of the received signals and a filter to reject the undesired frequency components. Because of the silent time, even for $\theta_i = \theta_0$ there are secondary harmonics that should be filtered. The amplitude at $\theta_i = 36$ is slightly smaller than at $\theta_i = 30$, and part of the energy is transferred to the first harmonic.

This result is critical, as it shows that an error in the scanned direction allows a correct reception of the transmitted signal at the cost of some gain loss (which is desired effect of a radiation pattern). For better illustration, refer to Figure 3.22 which shows the considered array radiation pattern. Finally, the amplitude loss at $\theta_i = 60$ is more severe as this angle falls within the sidelobe of the radiation pattern.

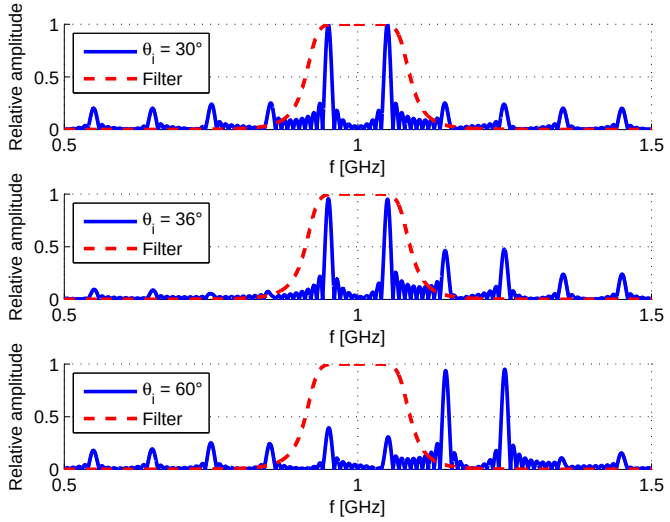

FIGURE 3.21: DSB received signal for $\theta_i = 30$, $\theta_i = 36$ and $\theta_i = 60$. The modulating signal is a 25 MHz pure tone and the carrier frequency is 1 GHz.

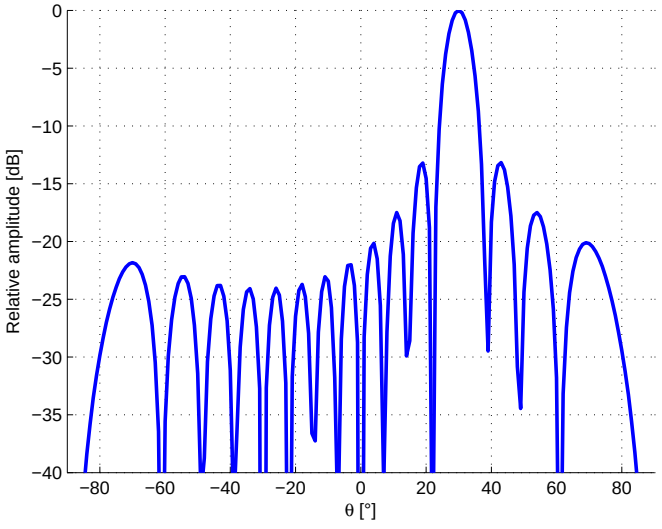

FIGURE 3.22: 4 element linear array scanned to $\theta_0 = 30$ radiation pattern.

According to Figure 3.21, it is possible to filter the main harmonic, return the signal to baseband and still recover the transmitted signal. This result is shown in Figure 3.23. The modulating signal is well recovered for $\theta_i = 30$ and $\theta_i = 36$, with an amplitude

difference because of the angle difference; and it is not recovered for $\theta_i = 60$. As a result, the bandwidth performance of the proposed technique is proved.

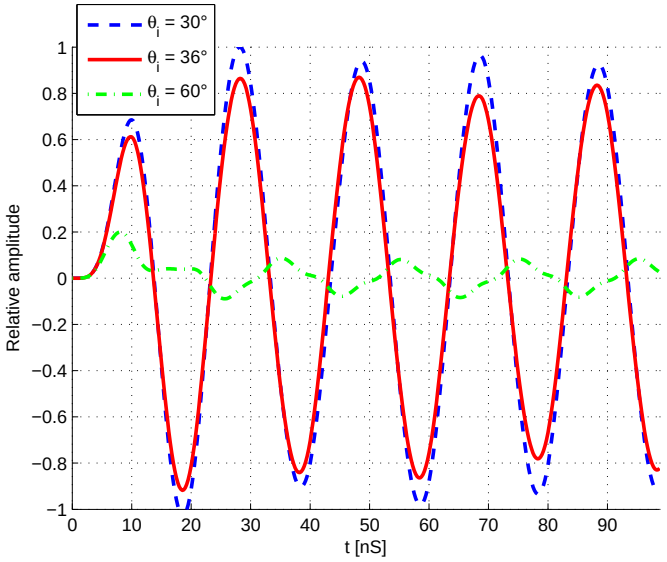

FIGURE 3.23: Recovered signal after filtering and baseband downconverting.

Chapter 4

Tapering effects

Contents

4.1 Introduction

Phased array antennas radiation pattern is directly related to each element weight and relative phase. The phase difference between elements sets the maximum radiation direction (the scanned direction) whilst the excitation coefficients amplitude defines the radiation pattern shape in terms of the main beam width and the SLL (sidelobe level). When the array elements are excited using a uniform amplitude relation, the SLL (the ratio between the main beam and the adjacent beam in a sinc function) is about 13.3 dB. This level, which may be very high for certain application that demand low sidelobes like radar, can be reduced by gradually decreasing the amplitude of the excitation coefficients. This process is known as tapering and it causes a radiation main beam widening in addition to the SLL reduction.

Tapering has been a widely studied area for many years and almost every book that covers phased array theory dedicates a section or a chapter to tapering study. In this Chapter, the effects of applying tappering to the technique proposed in Chapter 3 are

studied. For that purpose, coefficients obtained using a Gaussian distribution, as well as Dolph-Chebyshev and Taylor *N*-Bar series techniques will be applied as excitation terms. Dolph-Chebyshev and Taylor *N*-Bar series derivation can be found in [37] and [38].

The general procedure of this chapter is as follows:

- Three different tapering techniques will be considered: Gaussian distribution, Dolph-Chebyshev and Taylor *N*-Bar series.
- Each technique will be briefly introduced.
- Tapering effects will be shown by a collection of figures that simultaneously paint the received signal in the frequency domain for different incoming angles and the radiation pattern of the tapered array.

4.2 Gaussian tapering

Effects of tapering will be initially shown by exciting linear and planar array elements using a Gaussian distribution. For a N element planar array, whose elements are located over the x axis, spaced half a wavelength apart and centered in the origin, the excitation coefficients are given by the Gaussian distribution as:

$$f(x') = \frac{1}{\sqrt{2\pi\sigma^2}} e^{-\frac{1}{2}\left(\frac{x'}{\sigma\frac{(N-1)}{2}\frac{\lambda}{2}}\right)^2} = \frac{1}{\sqrt{2\pi\sigma^2}} e^{-8\left(\frac{x'}{\sigma(N-1)\lambda}\right)^2} \tag{4.1}$$

Where x' stands for antenna location over the x axis and σ is the standard deviation that characterizes the tapering.

4.2.1 Linear array

The easiest tapering example is given by a linear array. Figure 4.1 represents the effects of applying a Gaussian distribution described by $\sigma = 1$ to an eight-element linear array. Three different scenarios have been considered: $\theta_i = 0$, $\theta_i = 30$ and $\theta_i = 90$.

The bottom part of Figure 4.1 shows the radiation pattern comparison. Traditional phased array approach and the proposed technique are identical, as it can be concluded by comparing the solid blue line and the red circular points. In addition, the radiation pattern presents lower SLL and a wider main beam when the excitation coefficients

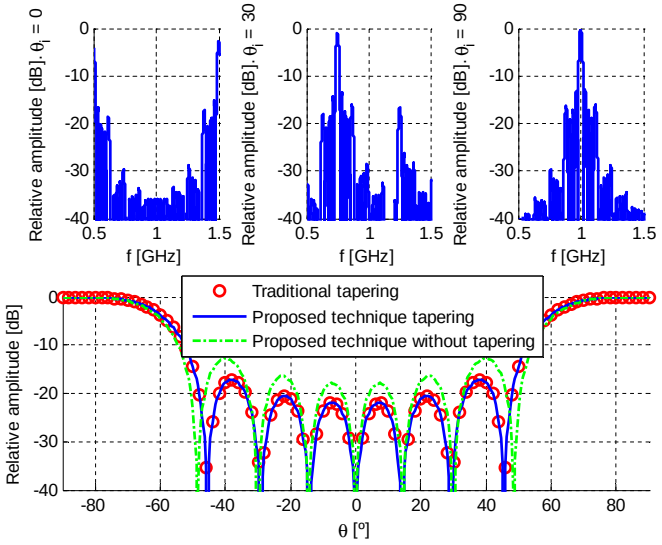

FIGURE 4.1: Received signal in frequency domain for three different incoming angles ($\theta_i = 0$, $\theta_i = 30$ and $\theta_i = 90$) and radiation pattern comparison. $\sigma = 1$, $\theta_0 = 90$

have been tapered (as was expected) The top part of Figure 4.1 shows the frequency shift produced by the angle mismatch produced when $\theta_i \neq \theta_0$. As the angle mismatch increases, the frequency shift gets higher. Another important relation is the received signal amplitude at 1 GHz, which is predicted by the radiation pattern since it is derived by taking the absolute value of the Fourier Transform at 1 GHz (the transmitted frequency).

4.2.2 Planar arrays

Gaussian tapering can be easily expanded to planar structures, since the Gaussian distribution fulfills the separable distribution condition. As a result, it is possible to apply the tapering independently in each dimension of the structure using the desired σ_x (tapering along x dimension) and σ_y (tapering along y dimension). An array located on the plane $z = 0$ has been assumed. Two different simulations have been done to validate Gaussian tapering in planar structures.

Figure 4.2 shows the radiation pattern and the received signal for a broadside 4×4 array after applying a symmetric Gaussian tapering defined by $\sigma_x = \sigma_y = 1$. Identical excitation coefficients have been applied in both dimensions, so the radiation pattern is the same in the principal cuts $\varphi = 0$ and $\varphi = 90$. The array has been simulated for three different incoming angles: $(\theta_i, \varphi_i) = (0, 0)$, $(\theta_i, \varphi_i) = (10, 0)$ and $(\theta_i, \varphi_i) = (30, 0)$. For $\theta_i = 30$ a replica of the transmitted signal (a pure tone) can be seen at $f = 1.0625GHz$. This frequency shift corresponds to the first harmonic, which can be derived as:

$$f_s = \frac{1}{T_s} = \frac{1}{N\left(t_s + \frac{d\sin\theta_0}{C}\right)} = 0.0625GHz \tag{4.2}$$

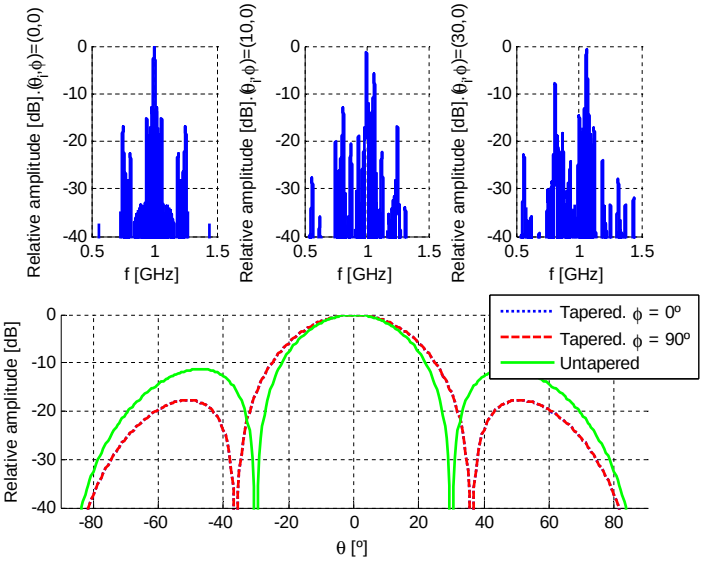

FIGURE 4.2: Received signal in frequency domain for three different incoming angles $(\theta_i, \varphi_i) = (0, 0)$, $(\theta_i, \varphi_i) = (10, 0)$ and $(\theta_i, \varphi_i) = (30, 0)$ and radiation pattern comparison. $\sigma_x = \sigma_y = 1$, $(\theta_0, \varphi_0) = (0, 0)$

Figure 4.3 considers the same situation as in Figure Figure 4.2 but an asymmetric tapering defined by $\sigma_x = 1$ and $\sigma_y = 0.8$ has been applied. Conclusions for Figure 4.3 are similar to those commented about Figure 4.2, the only difference is the variation in the principal cuts radiation pattern. Since the tapering is stronger in y dimension, the SLL is lower in the cut $\varphi = 90$. This result can be easily explained by the separable distribution properties. In the principal cut $\varphi = 0$, all the elements receive the same tapering in y dimension, so they are not affected by σ_y. In the principal cut $\varphi = 90$ the result is the same, but changing x and y roles.

4.3 Dolph-Chebyshev tapering

Dolph-Chebyshev generates the optimal taper excitation for a given SLL [39]. However, there is no gradual reduction in the SLL as the angle averts from the maximum radiation direction. Al the secondary lobes present the same relative level equal to SLL (generally given in dB). Doplh-Chebyshev excitation coefficients can be computed as follows [38]:

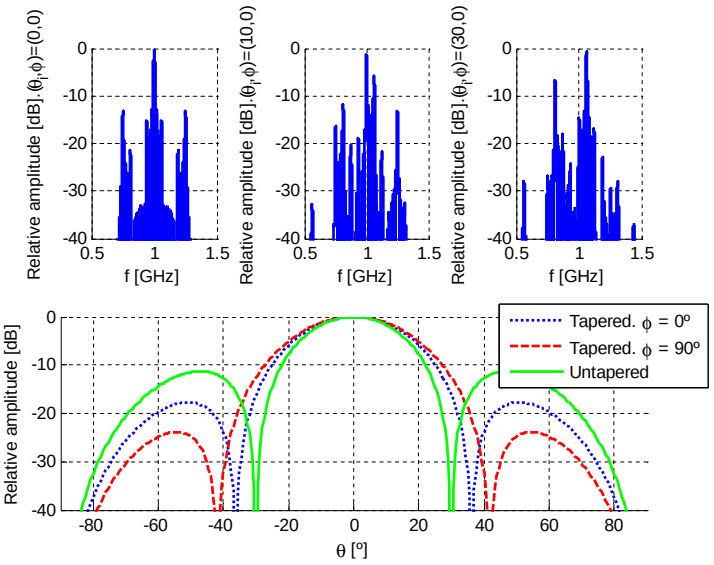

FIGURE 4.3: Received signal in frequency domain for three different incoming angles $(\theta_i, \varphi_i) = (0, 0)$, $(\theta_i, \varphi_i) = (10, 0)$ and $(\theta_i, \varphi_i) = (30, 0)$ and radiation pattern comparison. $\sigma_x = 1$, $\sigma_y = 0.8$, $(\theta_0, \varphi_0) = (0, 0)$

- Given the SLL (R), the array number of elements (N), a parameter c (do not confuse with light velocity) is defined as:

$$c = \frac{1}{2}\left[\left(R + \sqrt{R^2 - 1}\right)^{1/(N-1)} + \left(R - \sqrt{R^2 - 1}\right)^{1/(N-1)}\right] \tag{4.3}$$

- Given c, for N odd, the excitation coefficients are:

$$A_m = \sum_{i=1}^{N} T_{N-1}\left(c \cos\frac{\psi_i}{2}\right) \cos\left(m\psi_i\right) \tag{4.4}$$

  where $\psi_i = {}^{2\pi i}/_{N}$ and T_i is the Chebyshev polynomial of order i.

- For N even, the excitation coefficients are:

$$A_m = \sum_{i=1}^{N} T_{N-1}\left(c \cos\frac{\psi_i}{2}\right) \cos\left(\left(m - \frac{1}{2}\right)\psi_i\right) \tag{4.5}$$

- The excitation coefficients are symmetrical ($A_m = A_{-m}$), as a result, only half of the coefficients need to be computed. $A_m = 1$ stands for the array central element.

Dolph-Chebyshev results are shown in Figures 4.4 and 4.5. Figure 4.4 shows the radiation pattern at the received signal at three different incoming angles ($\theta_i = 0$, $\theta_i = 30$ and $\theta_i = 90$) for a broadside 16 element linear array with SLL = -20 dB. Figure 4.5

shows the same information for the same array scanned to $\theta_0 = 30$ and SLL = -25 dB. In both cases, the SLL adjusts to the desired value. In addition, it can clearly be seen the Dolph-Chebyshev synthesis property as all the side lobes take a constant value. The comparison to traditional array tapering is not shown, but both approaches are, again, identical.

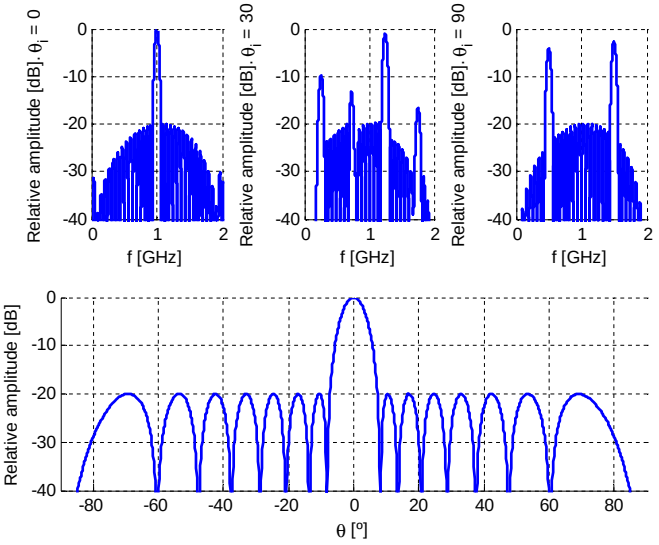

FIGURE 4.4: Received signal in frequency domain for three different incoming angles ($\theta_i = 0$, $\theta_i = 30$ and $\theta_i = 90$) and radiation pattern comparison. Dolph-Chebyshev tapering. SLL = -20 dB , $\theta_0 = 0$

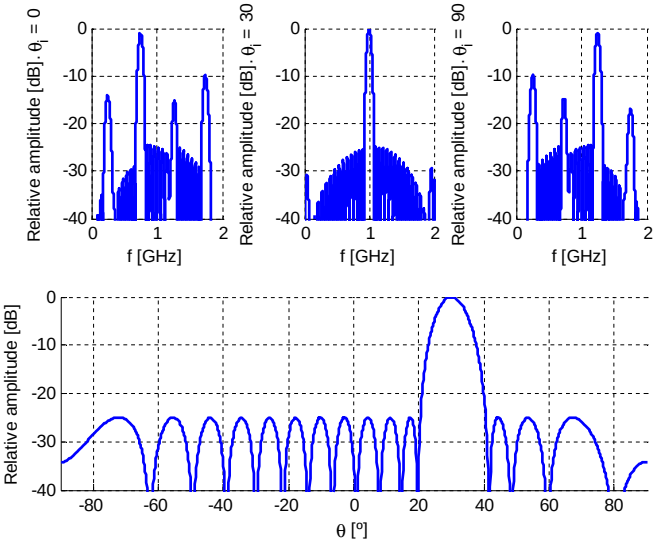

FIGURE 4.5: Received signal in frequency domain for three different incoming angles ($\theta_i = 0$, $\theta_i = 30$ and $\theta_i = 90$) and radiation pattern comparison. Dolph-Chebyshev tapering. SLL = -25 dB , $\theta_0 = 30$

4.4 Taylor *N*-Bar tapering

Dolph-Chebyshev presents constant sidelobe level. In case of large arrays, this constant level may suppose an important amount of reactive energy that will cause the system to be narrowband [36]. It is possible to overcome this issue by using techniques based on continuous distributions, like Taylor *N*-bar [40]. Taylor *N*-bar is a compromise between the constant sidelobe level obtained using Dolph-Chebyshev distribution and the $1/u$ falloff obtained with Taylor distribution with:

$$u = kdsin(\theta) \tag{4.6}$$

where k is the wave number and d is the element spacing ($\lambda/2$ in this case). Taylor coefficients can be easily obtained using the `taylorwin` command in Matlab.

Taylor *N*-bar synthesis technique is defined by two different parameters:

- SLL: Sidelobe maximum level
- $\tilde{n}$: Number of elements with no $1/u$ falloff

Figures 4.6 and 4.7 illustrate the effects of Taylor synthesis on the proposed technique (which are actually the same as in the traditional phased array approach).A 32 element linear array has been considered at both cases:

- Array at Figure 4.6 is scanned at $\theta_0 = 0$ and is defined by $(SLL, \tilde{n}) = (-20, 2)$
- Array at Figure 4.7 is scanned at $\theta_0 = 30$ and is defined by $(SLL, \tilde{n}) = (-25, 4)$

The frequency shift produced by the angle mismatch is more severe in Figures 4.6 and 4.7 than in Figures 4.4 and 4.5 because of the higher number of elements. An intuitive explanation can be given by observing both radiation patterns at the secondary lobe that the received angle falls within. Each secondary lobe displacement in the radiation pattern means a main harmonic located Ω_s away from the transmitted frequency. Since the array considered in Taylor examples is larger, its radiation pattern is more directive and as a result, an angle mismatch translates into a higher displacement in secondary lobes.

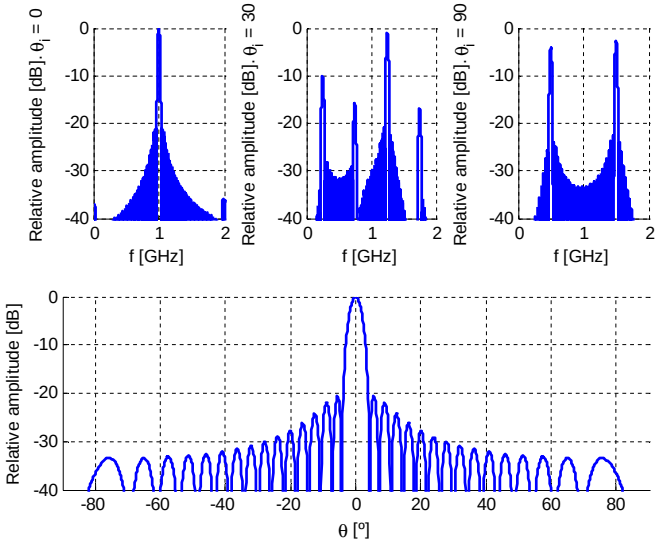

FIGURE 4.6: Received signal in frequency domain for three different incoming angles ($\theta_i = 0$, $\theta_i = 30$ and $\theta_i = 90$) and radiation pattern comparison. Taylor N-bar tapering. $(SLL, \tilde{n}) = (-20, 2)$, $\theta_0 = 0$

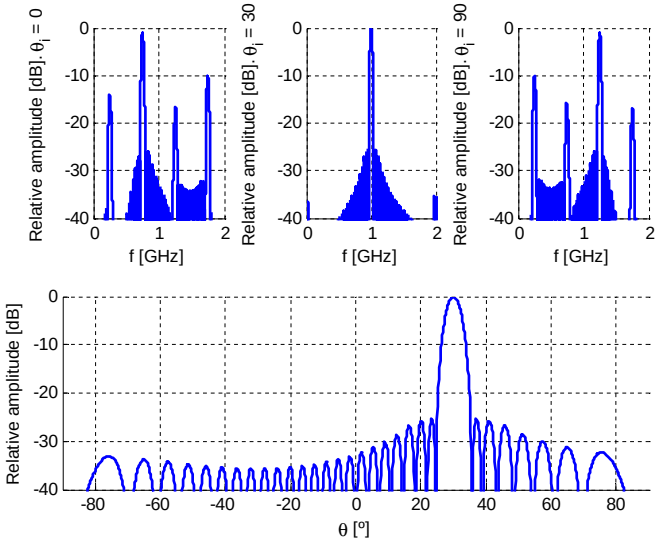

FIGURE 4.7: Received signal in frequency domain for three different incoming angles ($\theta_i = 0$, $\theta_i = 30$ and $\theta_i = 90$) and radiation pattern comparison. Taylor N-bar tapering. $(SLL, \tilde{n}) = (-25, 4)$, $\theta_0 = 30$

4.5 Technique comparison

To conclude the chapter, a comparison of the studied techniques will be done. A 16 element linear array has been tapered as follows:

- No tapering.
- Gaussian tapering defined by $\sigma = 1$.
- Dolph-Chebyshev defined by SLL = -20 dB.
- Taylor N-bar defined by (SLL, $\tilde{n}$) = (-20 dB,2).

A radiation pattern comparison is shown in Figure (4.8). The radiation patterns have been synthesized to present $SLL = -20$ in the first sidelobe. As it can be seen, only for Dolph-Chebyshev method this level remains constant. The constant value obtained with Dolph-Chebyshev causes the no tapered pattern to present lower sidelobes far from the scanned direction. The Gaussian tapering presents the highest SLL decrease. Taylor N-Bar shows an intermediate result, as sidelobes are located between Gaussian and Dolph-Chebyshev methods.

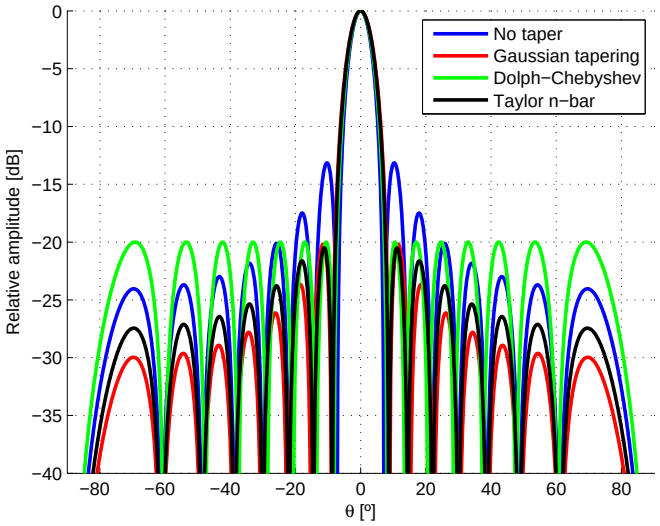

FIGURE 4.8: Comparison for Gaussian, Dolph-Chebyshev and Taylor N - Bar tapering

Chapter 5

Bandwidth enhancement

Contents

5.1 Introduction

Phased array theory is derived assuming a monochromatic plane wave. This assumption facilitates the problem analytic treatment but lacks of practical application, as a realistic RF signal must contain some bandwidth to transmit information. Phased array antennas whose performance is based on delay by phase shifting will be negatively affected by this bandwidth, since the time delay as a phase shift is only accurate in a

narrow band around the carrier frequency. Out of this band, the computed phase shift will not translate into the desired time delay and the constructive interference will not produce in the desired direction. As a consequence, each frequency will be scanned to a different direction producing an effect known as beam squint [41]. It is possible to overcome this situation by using true-time-delay shifter [42, 43], but these devices are complex and expensive.

The technique presented in Chapter 3 can be interpreted as a true-time-delay shifter, as the switching is controlled in the time domain and is independent of the frequency. However, as explained in section 3.4, the system bandwidth is limited by the number of antennas and the carrier frequency. According to (3.25) the maximum bandwidth for a 32 element array under a 1 GHz carrier is 20.833 MHz. In addition, this bandwidth is referred to the pass band bandwidth (refer to Figure 3.8 for better illustration), so the baseband bandwidth is approximately 10 MHz. For a 64 element array, this bandwidth gets reduced to 5 MHz. Furthermore, this bandwidth is derived assuming rectangular ideal filters, so the real bandwidth will be around a 25 % smaller. Hence, the practical system bandwidth is approximately 4 MHz for a 1 GHz carrier, which may not be wide enough for certain applications.

As a result, it becomes interesting to develop a method to increase this narrow bandwidth. In this chapter it is shown how to enhance the system bandwidth by optimizing the antenna sampling order.

5.2 Minimum delay, generic sampling order and arbitrary array definition

Chapter 3 theory has been derived using minimum delay sampling. Minimum delay sampling sequence is given by the order in which the received plane wave impinges the different array antennas, so the first element impinged is the first element sampled and the last element impinged is the last element sampled. As a result, the n+1 th antenna will always be able to sample the n+1th cycle thanks to the delay caused by the different space location (as it is depicted in Figure 3.1). There is only a situation in which there is no possibility of sampling the next cycle: when going back from the last antenna to the first one. This phenomenon has been described as silenced time.

On the other hand, there is not any reason that enforces the system to sample the array in minimum delay order. The proposed technique can be expanded to a generic order sampling, in other words, we can sample in whichever desired order. A comparison between minimum delay order and a generic sampling order is provided in Figure 5.1

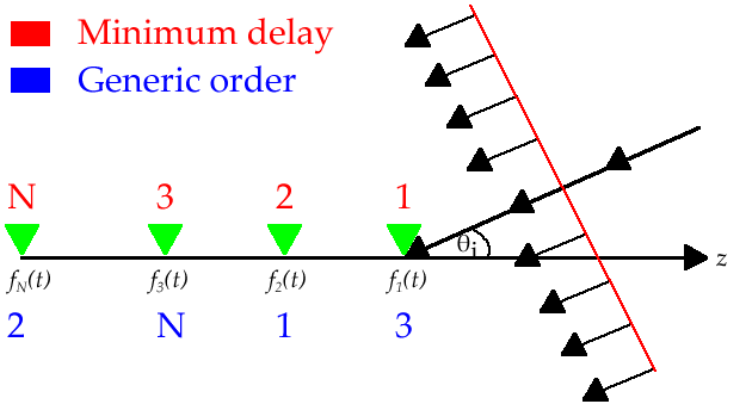

FIGURE 5.1: Comparison between minimum delay and generic sampling order

Generic sampling order complicates analytic analysis and invalidates the switching scheme proposed in Figure 3.4, which only holds for equally spaced linear arrays. Furthermore, there is neither any reason that enforces the system to be a linear equally spaced array (planar arrays have already been considered). In general terms, the set of antennas will be placed in arbitrary locations defined by $\vec{r_n}'$ as depicted in Figure 5.2

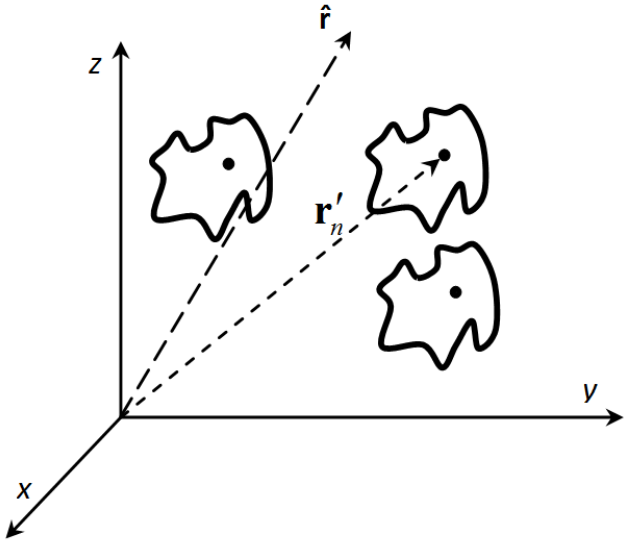

FIGURE 5.2: Arbitrary array where $\vec{r_n}'$ is the position of the n^{th} element and $\hat{r}$ can represent the direction of arrival or the scanned direction

Given this definition, it is necessary to develop a new sampling scheme. It is possible to generalize the technique proposed in Chapter 3 as follows:

I Receive a full cycle from the first antenna (which does not have to be the first impinged antenna) during t_s seconds

II Wait for $\Delta t_{1,2}$ seconds for the next cycle to arrive to antenna 2.

III Receive a full cycle from the second antenna

IV Wait for $\Delta t_{2,3}$ seconds for the next cycle to arrive to antenna 3.

V Repeat the procedure described in I-IV until reaching the last element. Then go back to the first antenna.

In general terms, the algorithm can be written as:

I Receive a full cycle from the n^{th} antenna during t_s seconds.

II Wait for $\Delta t_{n,n+1}$ seconds for the next cycle to arrive to antenna n+1.

III Receive a full cycle from the $n+1^{th}$ antenna.

The waiting time between the $n-1^{th}$ and the n^{th} antenna can be computed in a general form as:

$$\Delta t_{n-1,n} = \min \left[\frac{\left(\vec{r}_{n-1}' - \vec{r}_n'\right) \cdot \hat{r}_0}{c} - i_n t_s \right] > 0 \tag{5.1}$$

where $\hat{r}_0$ refers to the unit vector of the scanned direction pointing outwards and i_n is the number of full cycles that must be subtracted or added in order to assure causality ($\Delta t > 0$) as well as to avoid sampling twice the same cycle ($\Delta t < t_s$). As a result, a positive i_n means i_n lost cycles between the $n-1^{th}$ and the n^{th} antenna, whilst a negative i_n means that $|i_n|$ cycles must be waited to avoid sampling the same cycle twice. Equation (5.1) refers to the waiting time between two elements and it does include the special case of going back from the last antenna to the first one. In addition, by using (5.1) the system is not forced to sample the antennas in a periodic order.

5.3 Arbitrary array mathematical derivation

5.3.1 Time domain derivation

The formulation for an arbitrary array randomly sampled can be derived graphically. For this purpose, assume a 6 element array as the one shown in Figure 5.3.

This array receives a plane wave from a direction defined by $(\theta_i, \varphi_i) = (60, 0)$. Note that all the elements in the array are spaced a function of half a wavelength along the *x* axis. Half a wavelength for 60 degrees incidence corresponds to $\frac{T}{4}$ delay in time domain.

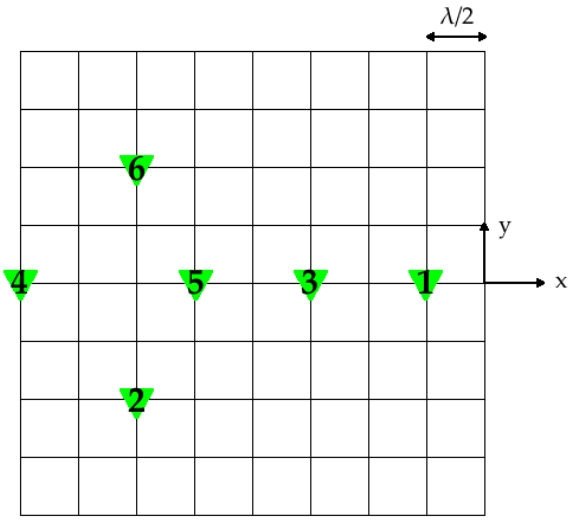

FIGURE 5.3: Array layout for graphical derivation. The array antennas are arbitrarily placed and impinged by a plane wave incoming from $(\theta_i, \varphi_i) = (60, 0)$. Each tile has $\lambda/2 \times \lambda/2$ dimensions

The received signal at the n^{th} antenna with respect to the first one (which is taken as phase reference) is:

$$f_{n,i} = f_0 \left(t + \frac{\left(\vec{r}'_n - \vec{r}'_1 \right) \cdot \hat{r}_i}{c} \right) \tag{5.2}$$

For the 6 element array considered in Figure 5.3, the signal received at each antenna is shown in Figure 5.4. Each cycle is labeled so that it is easier to establish when a cycle is lost or when it is necessary to wait before starting to sample.

By visual inspection of the cycle number, it is very easy to derive the sampled-lost-waited sequence as:

- Antenna 1 samples cycle 1.
- Antenna 2 waits for one cycle and samples cycle 2.
- Antenna 3 loses cycle 3 and samples cycle 4.
- Antenna 4 waits for one cycle and samples cycle 5.
- Antenna 5 loses cycle 6 and samples cycle 7.
- Antenna 6 samples cycle 8.
- Antenna 1 loses 2 cycles and samples cycle 11

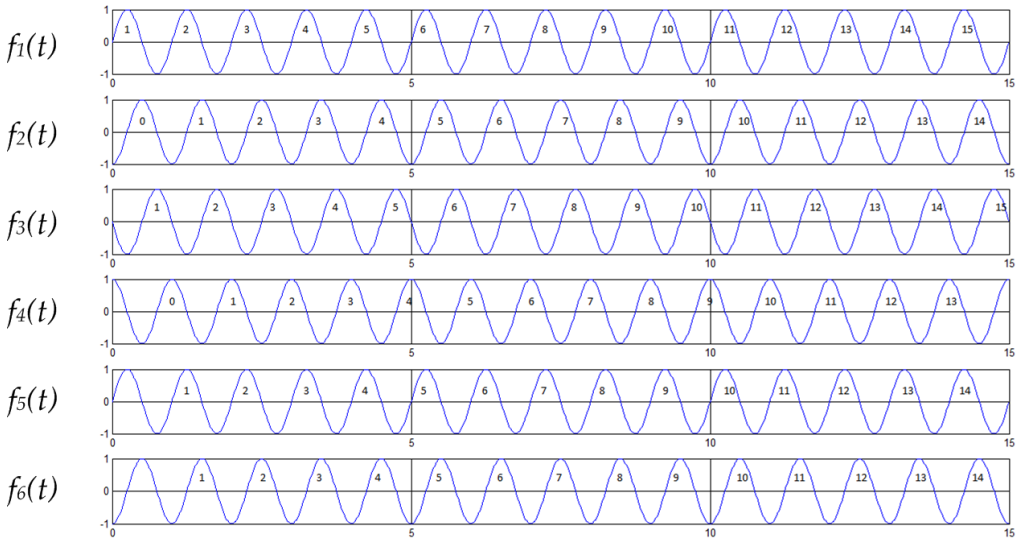

FIGURE 5.4: Received signals for the array shown in Figure 5.3.

- Repeat the process. The aperture period is 10 cycles.

An scheme for the sampled-lost-waited sequence is provided in Figure 5.5

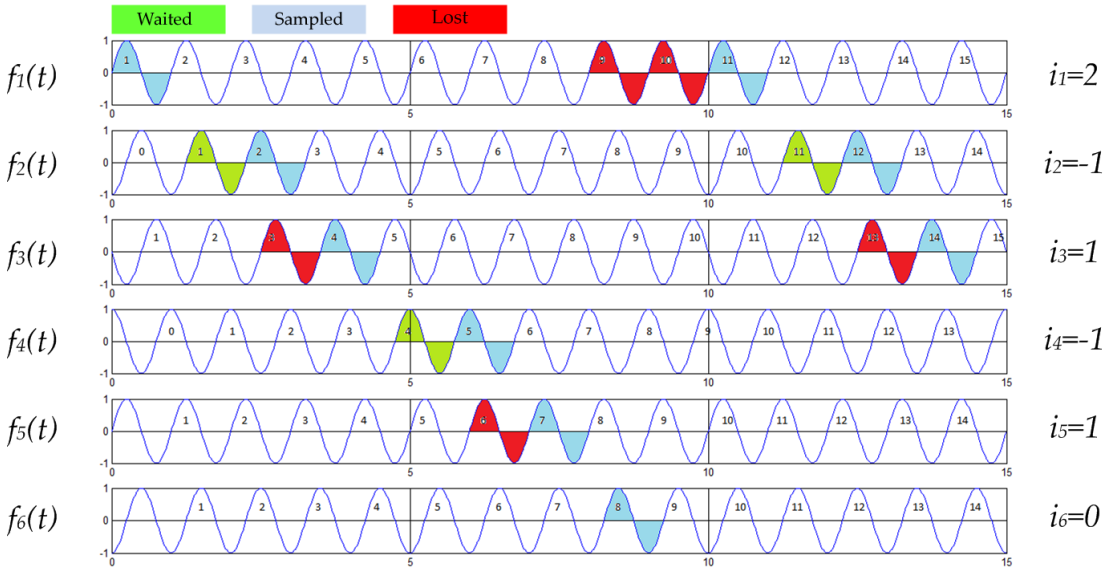

FIGURE 5.5: Sampled-lost-waited cycles for the array shown in Figure 5.3. The lost/waited cycles are correctly predicted by (5.1)

It is easy to derive an equation for the aperture sampling period as:

$$T_s = Nt_s + t_s \sum_{j=1}^{N} i_j \Gamma(i_j) \tag{5.3}$$

where $\Gamma(x)$ is the Heaviside step function.

The next step is to align all the signals. The alignment can be done in three different stages:

- Delay each each signal until being in phase with the last received signal:

$$f_n(t) = f_{n,i}\left(t - \sum_{m=n+1}^{N} \Delta t_{m-1,m}\right) \tag{5.4}$$

- Delay all the signals the maximum number of waited cycles:

$$f_n(t) = f_{n,i}\left(t - \sum_{m=n+1}^{N} \Delta t_{m-1,m} - t_s \max\left\{|i_m|\,\Gamma(-i_m)\right\}\right) \tag{5.5}$$

- Move forward those signals that have to wait any cycles:

$$f_n(t) = f_{n,i}\left(t - \sum_{m=n+1}^{N} \Delta t_{m-1,m} - t_s \left[\max\left\{|i_m|\,\Gamma(-i_m)\right\} - |i_n|\,\Gamma(-i_n)\right]\right) \tag{5.6}$$

The result of applying this alignment process to Figure 5.5 is shown in Figure 5.6.

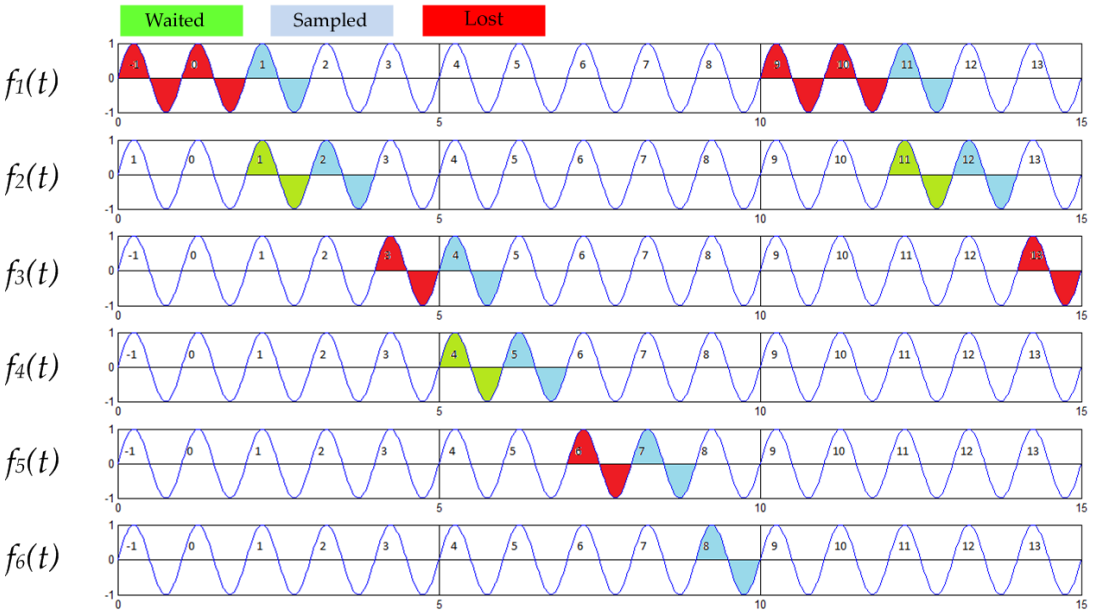

FIGURE 5.6: Aligned signals for the array shown in Figure 5.3.

The final step is to define the switching signals to window each antenna. If the signals are aligned like in Figure 5.6, the n^{th} antenna must sample the n+lost cyclesth cycle. In other words:

$$s_n(t) = \sum_{m=-\infty}^{\infty} \Pi\left(\frac{t-(n-1)t_s - t_s\sum_{j=1}^{n} i_j\Gamma(i_j) - mT_s}{t_s}\right) \tag{5.7}$$

The composed signal is the summation of the sampled signals:

$$f(t) = \sum_{n=1}^{N} f_n(t)\, s_n(t) \tag{5.8}$$

5.3.2 Spectral analysis

As in Chapter 3, Fourier Transform of (5.8) can be obtained as:

$$F(\omega) = \frac{1}{2\pi}\sum_{n=1}^{N} F_n(\omega) * S_n(\omega) \tag{5.9}$$

In order to make easier the derivation of (5.9), equations (5.6) and (5.7) can be rewritten as:

$$f_n = f_0(t + \Delta_{n,f}) \tag{5.10}$$

$$s_n(t) = \sum_{m=-\infty}^{\infty} \Pi\left(\frac{t - mT_s - \Delta_{n,s}}{t_s}\right) \tag{5.11}$$

where Δ_{nf} and Δ_{ns} are the delays applied to $f_n(t)$ and $s_n(t)$ respectively. Both parameters depend on the scanned direction defined by $\hat{r}_0$, the incoming direction defined by $\hat{r}_i$ and the array structure, which is defined by the matrix $\boldsymbol{R}$ as:

$$\mathbf{R} = \begin{bmatrix} r_{1x} & r_{1y} & r_{1z} \\ r_{2x} & r_{2y} & r_{2z} \\ \vdots & \vdots & \vdots \\ r_{Nx} & r_{Ny} & r_{Nz} \end{bmatrix} \tag{5.12}$$

By applying Fourier Transforms of (5.10) and (5.11) , (5.9) becomes:

$$F(\omega) = \frac{1}{2\pi} \sum_{n=1}^{N} \left(F_0(\omega) e^{j\omega\Delta_{n,f}} \right) * \left(\frac{2\pi t_s}{T_s} \sum_{m=-\infty}^{\infty} \operatorname{sinc}\left(\frac{m\pi t_s}{T_s} \right) \delta(\omega - m\Omega_s) \, e^{-jm\Omega_s\Delta_{n,s}} \right) \tag{5.13}$$

After applying the convolution operator and swapping the summation orders (so that the final equation is written as the sum of infinite harmonics) :

$$F(\omega) = \frac{t_s}{T_s} \sum_{m=-\infty}^{\infty} F_0(\omega - m\Omega_s) \sum_{n=1}^{N} \operatorname{sinc}\left(\frac{m\pi t_s}{T_s} \right) e^{j\omega\Delta_{n,f}} e^{-jm\Omega_s(\Delta_{n,s}+\Delta_{n,f})} \tag{5.14}$$

It is not possible to write a closed form solution for (5.14). However, it can rewritten as follows:

$$F(\omega) = \sum_{m=-\infty}^{\infty} F_0(\omega - m\Omega_s) a(m, R, \hat{r}_i, \hat{r}_0) \tag{5.15}$$

This result is equivalent to that obtained in (3.17) as the received signal is the summation of infinite frequency replicas spaced by the sampling rate Ω_s and weighted by an amplitude term denoted by $a(\cdot)$ (in (3.17) the function $a(\cdot)$ was a sinc function). This amplitude term is a function of the replica number (m), the array structure ($\boldsymbol{R}$) and the incoming and scanned angles ($\hat{r}_i, \hat{r}_0$). The sampling rate presents a dependence in the same factors as the amplitude.

Once again, a bandwidth limit can be derived as:

$$BW < \frac{\Omega_s}{2} \tag{5.16}$$

This limit is obtained by imposing no overlap between the main harmonic and the first replica of the received signal. However, if the amplitude of the first replica is under an established threshold (say -30 dB), the system bandwidth can be enhanced higher than the limit stated in (5.16)

5.4 Random periodic sampling

Given an arbitrary array defined whose scanned direction is defined by (θ_0, φ_0) and its matrix $\boldsymbol{R}$ (which is highly related to the sampling order), which is receiving a plane wave from (θ_i, φ_i), it is possible to predict the amplitude and location of the spectral components predicted by (5.15). However, there is no closed form equation and the only way to solve these values is by substituting all the unknowns in (5.14). This process may not be practical, since a heavy computational load is required.

An interesting alternative is to treat the term $a(\cdot)$ and the aperture sampling rate Ω_s as a random variable so the proposed technique is not deterministic anymore. In other words, given an array, its harmonics location and amplitude will be treated as random variables of the chosen sampling order.

To illustrate this result, assume a 12 element half a wavelength linear array. Figure 5.7 shows the spectrum of the received signal for two different order sequences. In both cases the transmitted signal is a pure tone at 1 GHz and $\theta_0 = \varphi_0 = 30$. Both executions present different spectral components. The first execution has less spacing between harmonics due to a lower aperture sampling rate, so the first harmonic is closer to the main harmonic. According to (5.16), this fact will make the first execution to present a lower bandwidth than the second one. However, the first harmonic relative amplitude at the first execution is approximately 10 dB smaller than in the second one. In addition the first harmonic amplitude is approximately 30 dB smaller than the main harmonic, hence it can be neglected yielding to a bandwidth that doubles the predicted by (5.16).

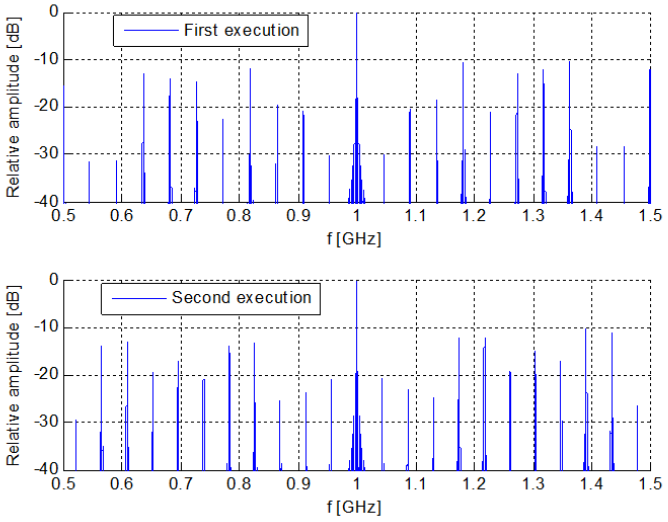

FIGURE 5.7: Spectrum comparison for two different sampling order sequences

One might think that the sampling order affects to the radiation pattern. Fortunately, this statement is not always true. For the considered case, the radiation pattern remains constant since the array is using the same unique information (in terms of delay difference between elements) independently from the sampling order. Hence, the random periodic sampling and the traditional phased array approach present identical radiation pattern, as shown in Figure 5.8.

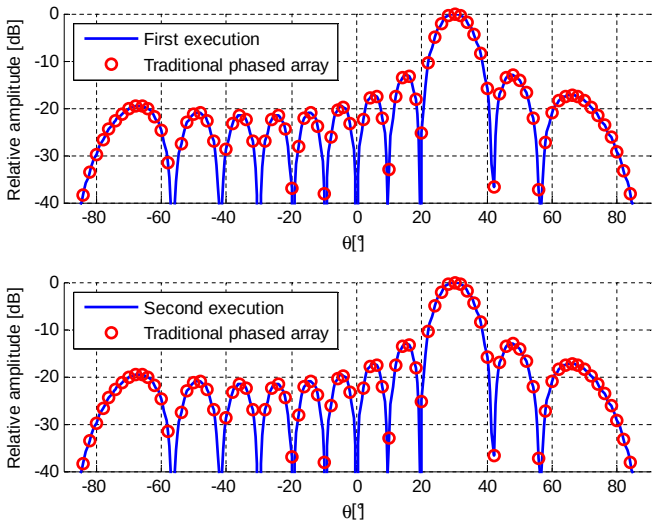

FIGURE 5.8: Radiation pattern comparison for two different sampling order sequences

As a result, it is important to choose an appropriate sampling order, since it will not affect to the phased array performance in terms of pattern, but it will allow a higher bandwidth. Two different optimization techniques are explained below: Backtracking and GA (Genetic Algorithm).

5.4.1 Backtracking optimization

Backtracking is a general algorithm to find **all** the solutions to some computational problem. It studies all the possible solutions and takes the best, or at least, it studies all the possible solutions until a stop criterion is reached.

Backtracking presents the following pros and cons:

- Pros: It is assured that the found solution is optimal.
- Cons: High computational cost, which can become just unaffordable as the problem size increases.

If the array is small ($N < 9$) it is possible to evaluate the $N!$ possible combinations and select the best one. For that purpose, it is necessary to define which is the best solution. Since we are interested in enhancing the system bandwidth, the best solution is the one that presents a higher bandwidth with harmonics below a threshold. The results presented for this technique, as well as the GA, have been computed with a threshold of -30 dB.

As a consequence of the $a(\cdot)$ dependence on the array structure, the incoming and scanned direction, the sampling order must be optimized for each (θ_0, φ_0) direction.

Tables 5.1 and 5.2 show the bandwidth enhancement for a linear array as a function of the number of elements for two different scanned directions: $(\theta_0, \varphi_0) = (30, 0)$ and $(\theta_0, \varphi_0) = (60, 0)$. In both cases, the linear array is placed along the x axis and its elements are spaced half a wavelength apart. In addition, a 1 GHz pure tone is the transmitted signal. The original bandwidth is given by minimum delay sampling, as this is the natural sampling order.

TABLE 5.1: Bandwidth enhancement using backtracking. $(\theta_0, \varphi_0) = (30, 0)$

N	Original bandwidth (MHz)	Harmonics down threshold	Bandwidth after optimization (MHz)
4	100	1	166.67
5	83.33	0	83.33
6	62.5	2	166.67
7	55.56	1	83.33
8	50	3	166.67

TABLE 5.2: Bandwidth enhancement using backtracking. $(\theta_0, \varphi_0) = (60, 0)$

N	Original bandwidth (MHz)	Harmonics down threshold	Bandwidth after optimization (MHz)
4	83.33	1	166.67
5	71.43	0	71.43
6	55.56	2	125
7	50	1	83.33
8	41.67	3	125

The bandwidth enhancement improves as the number of elements increases and seems to work better for even number of elements than for odd. Graphic results are shown in Figure 5.9, which shows a comparison between minimum delay bandwidth and optimized bandwidth for $N = 6$ and $N = 8$.

The computational cost can be appreciated in the total simulation time. For $N = 8$ it takes around an hour to complete the simulation using a VTAG lab computer (2.6GHz processor). For $N = 9$ the simulation time increases to approximately 10 hours since

the backtracking complexity for a permutation problem is $O(N!)$. As a result, for $N = 12$, the simulation is expected to last for more than two years. Hence, an alternative method is required for large arrays.

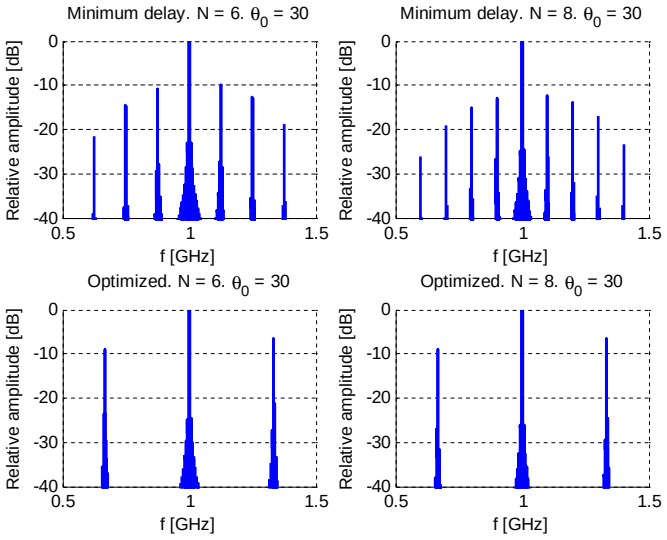

FIGURE 5.9: Bandwidth enhancement using backtracking optimization

5.4.2 Genetic algorithm optimization

An alternative to backtracking optimization for large problems is Genetic Algorithms (GA) [44, 45]. GA presents an affordable complexity ad its simulation time can be controlled. As a negative point, GA does not explore all the possible combinations and it does not provide any guarantee that the final solution is optimum. General theory about GA and about the actual problem representation is provided in Appendix A.

Table 5.3 shows the bandwidth enhancement for a linear array, $\lambda/2$ uniformly spaced after running the genetic algorithm. The array is scanned to $(\theta_0, \varphi_0) = (30, 0)$. Information from Table 5.3 is complemented with Figure 5.10, which shows a comparative between minimum delay bandwidth and GA optimization for N = (10,12,14,16)

5.4.3 Random periodic optimization conclusion

By combining results in Tables 5.1, 5.2 and 5.3 it is possible to obtain some intuitive conclusions:

- The bandwidth enhancement works better for even number of elements.

TABLE 5.3: Bandwidth enhancement using a genetic algorithm. $(\theta_0, \varphi_0) = (30, 0)$

N	Original bandwidth (MHz)	Harmonics down threshold	Bandwidth after optimization (MHz)
9	45.45	2	100
10	38.46	4	125
11	35.71	2	88.23
12	33.33	5	125
14	27.78	4	104.16
16	25	4	80.65

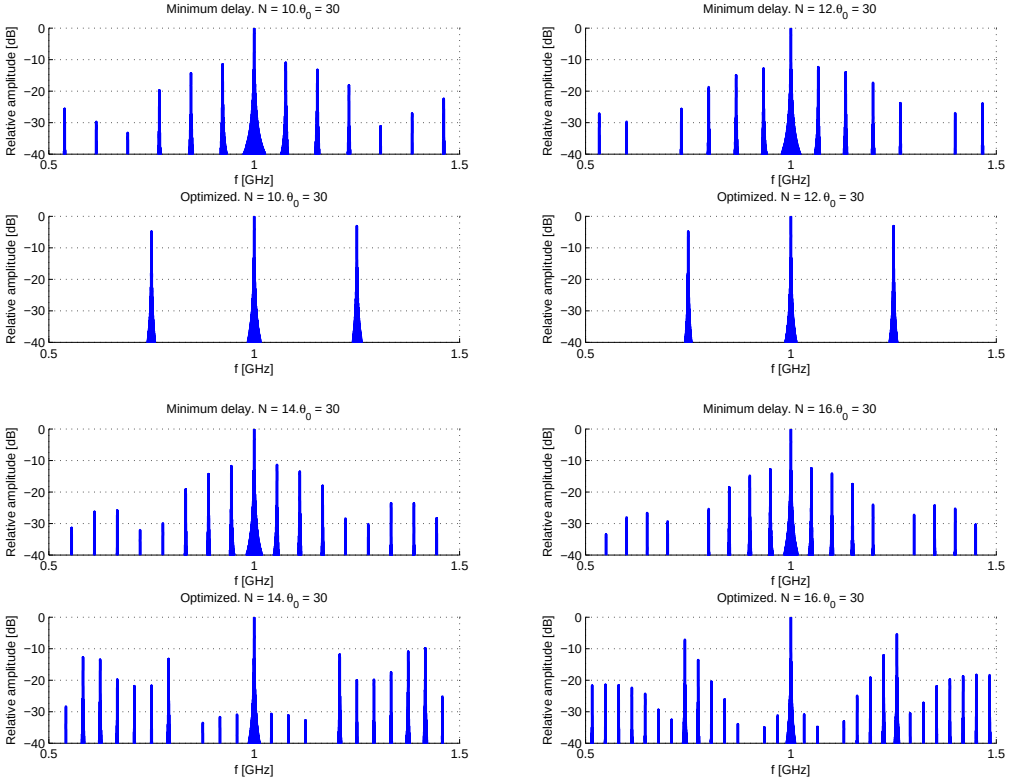

FIGURE 5.10: Bandwidth enhancement using genetic algorithm for N = (10,12,14,16)

- The decrease in the minimum delay bandwidth is faster than in the enhanced bandwidth.
- There is a tendency in the number of harmonics down the threshold for larger arrays that is broken for $N > 12$.
- For $N > 12$, the GA might not have obtained the optimum result

5.5 Maximum delay sampling

There is one situation in which (5.14) is analytically solvable: Maximum delay sampling. Maximum delay sampling is defined as the inverse order of Minimum delay sampling. In other words, the first antenna to sample is the last one in the impinging wave propagation path, the second antenna to sample is the second last one in the impinging wave propagation path and so forth. For this sampling scheme, the received signal is independent from the array structure and received angle if the distance between any two consecutive antennas is less than a wavelength. Figure 5.11 shows the maximum delay received signal for a 4-element array. After each sampled cycle there is a silenced cycle. This result is explained by (5.1) as follows: when moving from the n^{th} antenna to the $n+1^{th}$ antenna it will be always necessary to add a full cycle to make $\Delta t_{n,n+1}$ positive. In addition, i_n cannot be greater than one since the distance between consecutive elements has been restricted to be smaller than a wavelength. The only case when $i_n \neq 1$ is for $n = 1$ which is the switch between the last antenna and the first one (in this case $i_1 = 0$).

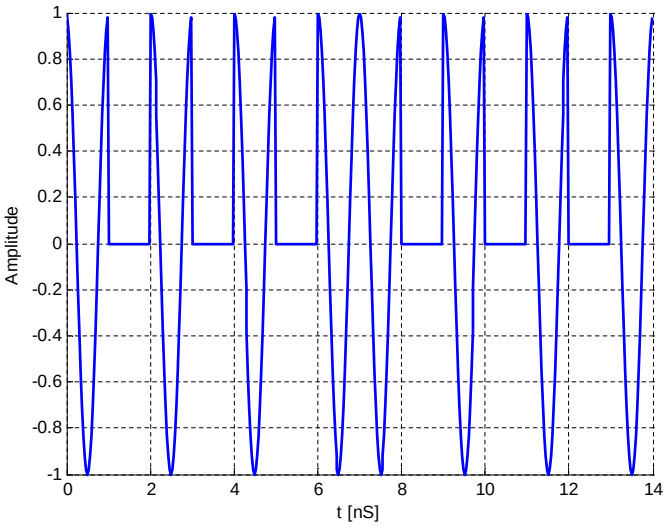

FIGURE 5.11: Example of received signal using maximum delay signal for 4-element array. The trasmitted signal is a 1 GHz tone. The array layout is 4 element $\lambda/2$ spaced.

5.5.1 Mathematical derivation

Assume an N-element linear array, whose elements are equally spaced along the z axis as shown in Figure 5.12. This structure receives a plane wave with direction θ_i. Taking the first antenna as a reference, the received signal at the n^{th} antenna is:

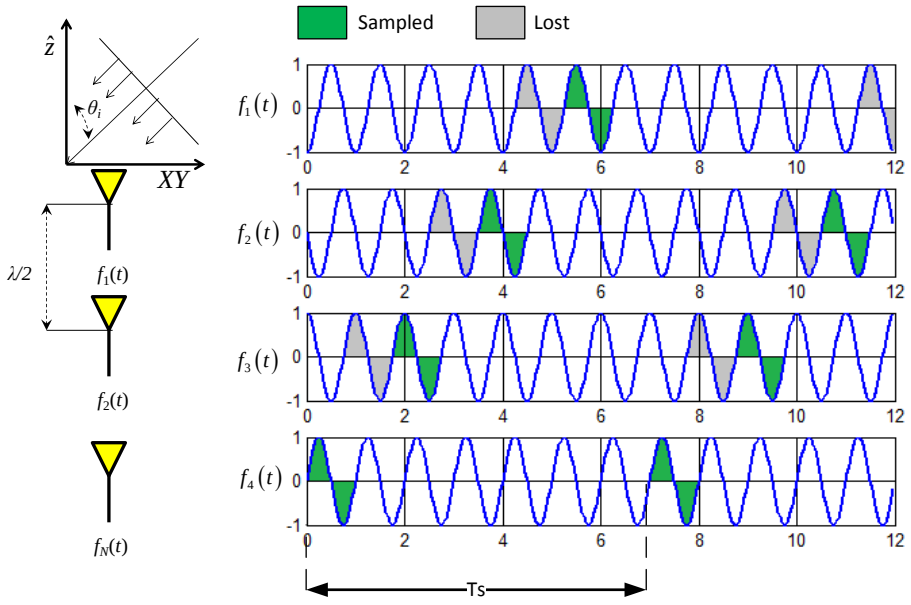

FIGURE 5.12: Maximum delay scheme. Example for $N = 4$

$$f_n(t) = f_0\left(t - t_s(n-1)\frac{\cos\theta_i}{2}\right) \tag{5.17}$$

Without loss of generality let $0 < \theta_i < 90$. As a result, the first antenna to be sampled is the N^{th} one. The second one is $N-1^{th}$ and so forth. According to Figure 5.11 there will be a loss cycle in each $n, n+1$ transition except when going from the last antenna to the first one. Using this information, the switching signal can be defined as:

$$s_n(t) = \sum_{m=-\infty}^{\infty} \Pi\left(\frac{t - (n-1)\frac{t_s\cos\theta_0}{2} - 2(N-n)t_s - mT_s}{t_s}\right) \tag{5.18}$$

The aperture sampling period is the sum of the sampled cycles (N) and the loss cycles ($N-1$), yielding:

$$T_s = (2N-1)t_s \tag{5.19}$$

The gathered signal is the sum of the windowed received signals after removing the relative delays as:

$$f(t) = \sum_{n=1}^{N} (f_n(t)\, s_n(t)) * \delta\left(t - (N-n)\frac{d\cos\theta_0}{C}\right) \tag{5.20}$$

As usual, it is interesting to study the received signal in the frequency domain:

$$F(\omega) = \frac{1}{2\pi} \sum_{n=1}^{N} \left(F_n(\omega) * S_n(\omega) \right) e^{-j\omega(N-n)\frac{d\cos\theta_0}{C}} \tag{5.21}$$

$F_n(\omega)$ and $S_n(\omega)$ can be computed as in Chapter 3 and substituted in (5.21) as:

$$\begin{aligned} F(\omega) = \tfrac{t_s}{T_s} \sum_{n=1}^{N} e^{-j\omega(N-n)\frac{t_s\cos\theta_0}{2}} \left(F_0(\omega)\, e^{-j\omega(n-1)\frac{t_s\cos\theta_i}{2}} \right) \\ * \left(\sum_{m=-\infty}^{\infty} sinc\left(\tfrac{m\pi t_s}{T_s}\right) \delta\left(\omega - \tfrac{2m\pi}{T_s}\right) e^{-j\frac{2m\pi t_s}{T_s}\left((n-1)\frac{\cos\theta_0}{2}+2(N-n)\right)} \right) \end{aligned} \tag{5.22}$$

After applying convolution and swapping summation order, (5.22) becomes:

$$\begin{aligned} F(\omega) = \tfrac{t_s}{T_s} e^{-j\omega(N-1)\frac{t_s\cos\theta_0}{2}} \sum_{m=-\infty}^{\infty} e^{-j\frac{4m\pi t_s}{T_s}(N-1)} \\ \cdot sinc\left(\tfrac{m\pi t_s}{T_s}\right) F_0(\omega - m\Omega_s) \sum_{n=1}^{N} e^{j(n-1)t_s\psi} \end{aligned} \tag{5.23}$$

In this case, ψ stands for:

$$\psi = t_s \left[\frac{\omega}{2} (\cos\theta_0 - \cos\theta_i) + \frac{m\pi}{T_s} (4 + \cos\theta_i - \cos\theta_0) \right] \tag{5.24}$$

Summation in (5.23) can be solved to rewrite the equation as:

$$\begin{aligned} F(\omega) = \tfrac{t_s}{T_s} e^{-j\omega(N-1)\frac{t_s\cos\theta_0}{2}} e^{j\frac{\psi}{2}(N-1)} \\ \cdot \sum_{m=-\infty}^{\infty} e^{-j\frac{4m\pi t_s}{T_s}(N-1)} sinc\left(\tfrac{m\pi t_s}{T_s}\right) F_0(\omega - m\Omega_s) \tfrac{\sin(\frac{N\psi}{2})}{\sin(\frac{\psi}{2})} \end{aligned} \tag{5.25}$$

This equation is again equivalent to the traditional phased array filter if filtered around $m = 0$.

Finally, consider the case when $\theta_i = \theta_0$, hence:

$$\psi = \frac{4m\pi t_s}{T_s} \tag{5.26}$$

By substituting (5.26) in (5.25):

$$F\left(\omega,\theta_i=\theta_0\right)=\frac{t_s}{T_s}\sum_{m=-\infty}^{\infty}e^{-j\omega(N-1)\frac{t_s\cos\theta_0}{2}}e^{j\frac{2m\pi}{2N-1}(N-1)} \cdot sinc\left(\frac{m\pi}{2N-1}\right)\frac{\sin(\frac{2mN\pi}{2N-1})}{\sin(\frac{2m\pi}{2N-1})}F_0\left(\omega-m\Omega_s\right) \tag{5.27}$$

As usual, the received signal is the summation of infinite frequency replicas spaced Ω_s in frequency. In this case, the amplitude of each replica is given by:

$$a(m)=sinc\left(\frac{m\pi}{2N-1}\right)\frac{\sin(\frac{2mN\pi}{2N-1})}{\sin(\frac{2m\pi}{2N-1})} \tag{5.28}$$

Figure 5.13 shows a graphic representation of (5.28) for an N-element array, with $N=(16,32,64,100)$. The representation is done as follows:

- In abscissa: the harmonic replica normalized to the number of array elements m/N.
- In ordinate: the amplitude of the harmonic split in the two different factors that can be seen in (5.28).

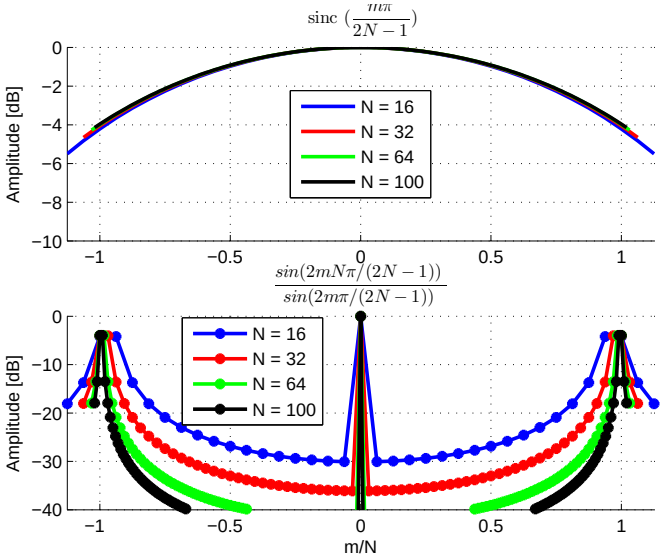

FIGURE 5.13: Graphic study of (5.28)

Although the first factor remains constant with the number of elements, the second one presents a very interesting behavior: As the number of elements in the array increases, the harmonic amplitude gets reduced below the -30 dB threshold except for $m\simeq N$. As

a result, up to $N-1$ harmonics can be neglected in a enough large array yielding the following bandwidth:

$$BW = \frac{N}{2T_s} = \frac{N}{2\,(2N-1)\,t_s} \simeq \frac{f}{4} \tag{5.29}$$

Hence, for a enough large array, the system bandwidth is approximately one fourth of the carrier frequency, independent of the scanned angle, the number of elements and their layout. Simulation evidence of this statement is provided in the next section.

5.5.2 Simulation

After analytically deriving maximum delay performance in section 5.5.1, a simulation evidence is given below. Two different simulations are presented:

- Figure 5.14: Harmonic amplitude as a function of the array number of elements. An N-element linear array, with $N = (16, 32, 64, 100)$, scanned to $(\theta_0, \varphi_0) = (30, 0)$ is considered. The incoming signal is a pure 1 GHz tone from $(\theta_i, \varphi_i) = (\theta_0, \varphi_0)$ The goal of this simulation is to show the convergence of the sampling technique bandwidth to one fourth of the carrier frequency.

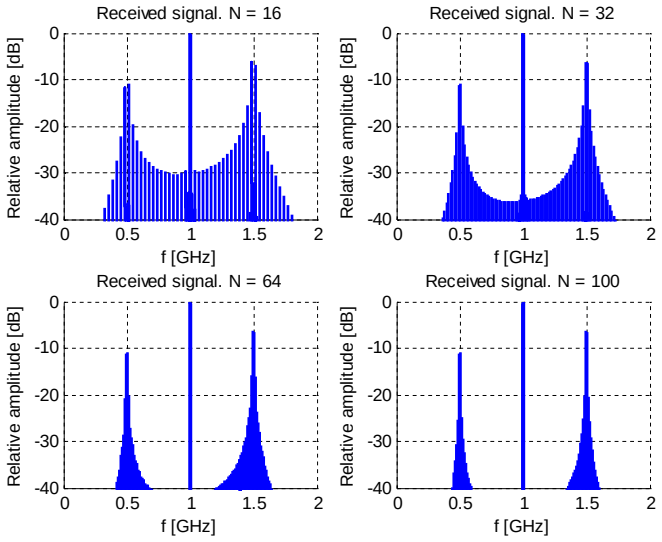

FIGURE 5.14: Received signal as a function of the number of elements using maximum delay sampling

- Figure 5.15: Harmonic amplitude as a function of the scanned direction and the array layout. A 16 element array with two different configurations (linear 16×1

and planar 4×4) scanned to two different directions ($(\theta_0, \varphi_0) = (30, 30)$ and $(\theta_0, \varphi_0) = (20, 10)$) has been considered. The goal of this simulation is to show the non dependence of the received signal on the array layout and the scanned direction.

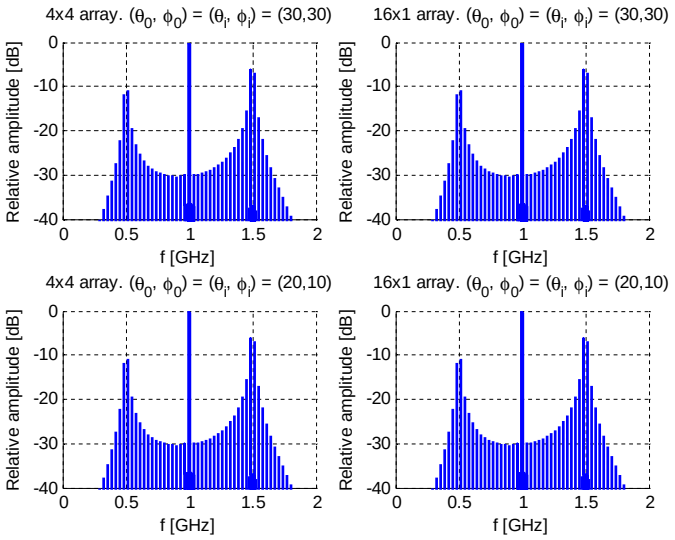

FIGURE 5.15: Received signal as a function of the array layout and the scanned direction using maximum delay sampling

5.6 Non periodic sampling

So far, a periodic sampling sequence has been assumed. This sampling sequences yields to the presence of secondary harmonics at frequencies that are multiple of the aperture sampling rate. It seems a good idea to suppress the periodicity in the sampling order sequence, or in other words, extend the aperture sampling period up to infinity.

A mathematical formulation can be derived using the same waiting time principle as previously in this Chapter. Since there will be no periodicity in the switching signal, it will not be possible to align the signals by delaying each antenna a constant amount of time. In contrast, the formulation will be derived assuming the possibility of moving forward signals. This idea, which at first glance breaks causality rules, can be applied since the sampled information will be transferred to a DSP or other processing unit with some delay.

Let an antenna located at $\vec{r}_1'$ to received a signal $f_1(t)$ which will be considered as reference:

$$f_1(t) = f_{1,i}(t) = f_0(t + \frac{\vec{r}_1' \cdot \hat{r}_i}{c}) \tag{5.30}$$

Let a second antenna located at $\vec{r}_2'$ whose received signal is:

$$f_{2,i}(t) = f_0(t + \frac{\vec{r}_2' \cdot \hat{r}_i}{c}) \tag{5.31}$$

It is possible to align (5.30) and (5.31) as:

$$f_{_2}(t) = f_0(t + \frac{\vec{r}_2' \cdot \hat{r}_i}{c} + \frac{(\vec{r}_1' - \vec{r}_2') \cdot \hat{r}_0}{c}) = f_{_1}(t) \quad if \quad \hat{r}_i = \hat{r}_o \tag{5.32}$$

A third signal described by:

$$f_{3,i}(t) = f_0(t + \frac{\vec{r}_3' \cdot \hat{r}_i}{c}) \tag{5.33}$$

Can also be aligned as

$$f_3(t) = f_0(t + \frac{\vec{r}_3' \cdot \hat{r}_i}{c} + \frac{(\vec{r}_1' - \vec{r}_3') \cdot \hat{r}_0}{c}) = f_0(t + \frac{\vec{r}_3' \cdot \hat{r}_i}{c} + \frac{(\vec{r}_2' - \vec{r}_3') \cdot \hat{r}_0}{c} + \frac{(\vec{r}_1' - \vec{r}_2') \cdot \hat{r}_0}{c}) \tag{5.34}$$

In this case, we are adding the waiting time for the second and the third signal. This waiting time is very similar to that predicted by (5.1). The only difference in this case is the possibility of going back and forth in time. For the n^{th} antenna:

$$f_n(t) = f_0(t + \frac{\vec{r}_n' \cdot \hat{r}_i}{c} + \sum_{j=1}^{n} \Delta t_{j-1,j}) \tag{5.35}$$

If causality is enforced, (5.1) can be applied to derive $\Delta t_{j-1,j}$. Hence, it is possible to adapt (5.35) to (5.6) and (5.7) to derive the formulation for no periodic sampling. The composed signal can be written as:

$$f(t) = \sum_{n=1}^{N} f_n(t) \cdot \Pi \left(\frac{t - (n-1)t_s - t_s \sum_{m=1}^{n} i_m \Gamma(i_m)}{ts} \right) \tag{5.36}$$

where

$$f_n(t) = f_{n,i}\left(t + \sum_{j=1}^{n} \Delta t_{j-1,j} - t_s\left[\max\left\{|i_m|\,\Gamma(-i_m)\right\} - |i_n|\,\Gamma(-i_n)\right]\right) \tag{5.37}$$

$$f_{n,i}(t) = f_0\left(t + \frac{\vec{r}_n \cdot \hat{r}_i}{c}\right) \tag{5.38}$$

It is also possible to write as a function of $f_0(t)$

$$f_n(t) = f_0\left(t + \delta_n\right) \tag{5.39}$$

$$\delta_n = \mathrm{mod}\left(\frac{\vec{r}_n \cdot \hat{r}_i}{c} + \sum_{j=1}^{n} \Delta t_{j-1,j}, t_s\right) - t_s\left[\max\left\{|i_m|\,\Gamma(-i_m)\right\} - |i_n|\,\Gamma(-i_n)\right] \tag{5.40}$$

Finally, the phase difference between the first and the last impinged elements (δ_{MAX}) can be deleted, so all the elements but the last one are delayed, and as a result, causality is fulfilled:

$$f(t) = \sum_{n=1}^{N} f_n(t - \delta_{MAX}) \cdot \Pi\left(\frac{t - (n-1)t_s - t_s \sum_{m=1}^{n} i_m \Gamma\left(i_m\right)}{ts}\right) \tag{5.41}$$

Based on this approach, two different sampling techniques have been considered: random aperiodic sampling and group periodic sampling.

5.6.1 Random aperiodic sampling

Random aperiodic sampling is defined as follows:

- Randomly pick one antenna and sample it.
- Randomly select a new antenna without taking in consideration which antennas have been previously selected.

A direct consequence of this sequence order is that all antennas can be selected with a probability of $1/N$ at each instant. On the other hand, the radiation pattern will not be identical to the traditional phased array approach, since some antennas will be used more often than others.

Random aperiodic sampling performance is shown in Figures 5.16 and 5.17. Figure 5.16 shows the radiation pattern and the received signal after taking 500 cycles. Figure

5.17 does the same for 5000 cycles. It is important to mention the random properties of this approach, so both Figures are likely to be different at each execution.

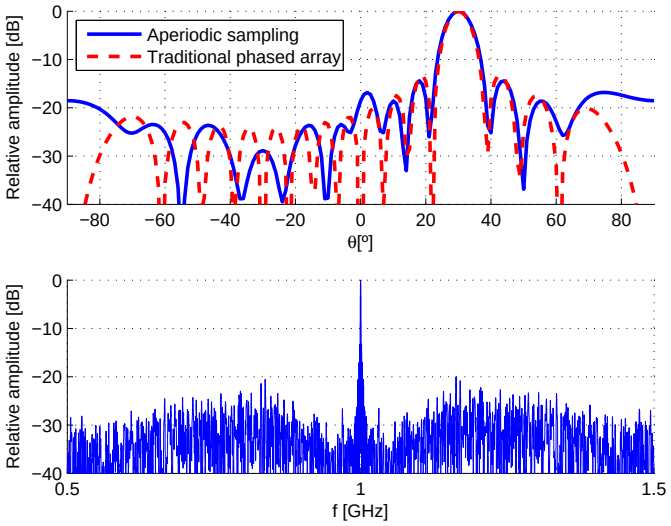

FIGURE 5.16: Received signal and radiation pattern using random aperiodic sampling after 500 cycles

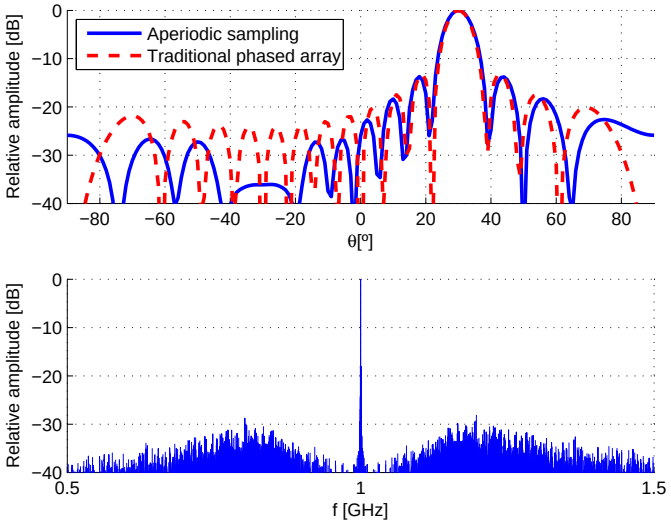

FIGURE 5.17: Received signal and radiation pattern using random aperiodic sampling after 5000 cycles

As it can be seen, the radiation pattern is no longer identical to the traditional phased array approach. However, as the number of cycles increases both the random aperiodic radiation pattern tends to the traditional phased approach one. In addition, the main beam and the two first sidelobes are almost identical, so in terms of radiated energy,

most part of it will be radiated in the same way as in the traditional phased array approach.

Another interesting result is the no presence of harmonics. Instead, the received signal presents some background noise that reduces as the number of received cycles increases.

According to the results in Figures 5.16 and 5.17, it is expected that for a enough large number of cycles the radiation pattern for this sampling scheme is identical to the traditional phased array one and the background noise disappears.

5.6.2 Group aperiodic sampling

Periodic sampling presents identical radiation pattern to traditional phased array approach, but it is limited in the number of elements by the carrier to signal bandwidth ratio. Random aperiodic sampling gets rid of secondary harmonics but its radiation pattern is slightly different to the traditional phased array approach. It is possible to combine the benefits from both methods using group aperiodic sampling.

The translation from harmonics to background noise is given by the aperiodic sampling sequence. On the other hand, the radiation pattern identical to traditional phased array approach is given by using all the array elements with the same frequency. Hence, an aperiodic sampling sequence that presents the same usage frequency for all the elements will yield the desired sampling technique. This sampling technique receives the name group periodic sampling and is defined as follows:

- Generate a random permutation of the N array elements and sample the array.
- Generate a new random permutation and sample again.

In other words, the sampling sequence is composed of infinite sub-sequences of N elements that only include each antenna once.

Random aperiodic sampling performance is shown in Figures 5.18 and 5.19. Figure 5.18 shows the radiation pattern and the received signal after taking 500 cycles. Figure 5.19 does the same for 5000 cycles.

As expected, the radiation pattern is identical to the traditional phased array approach and the received signal presents a similar behavior to Figures 5.16 and 5.17.

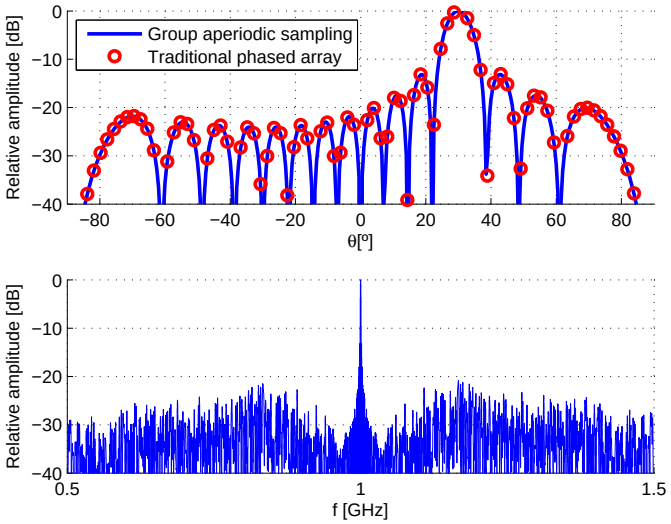

FIGURE 5.18: Received signal and radiation pattern using group aperiodic sampling after 500 cycles

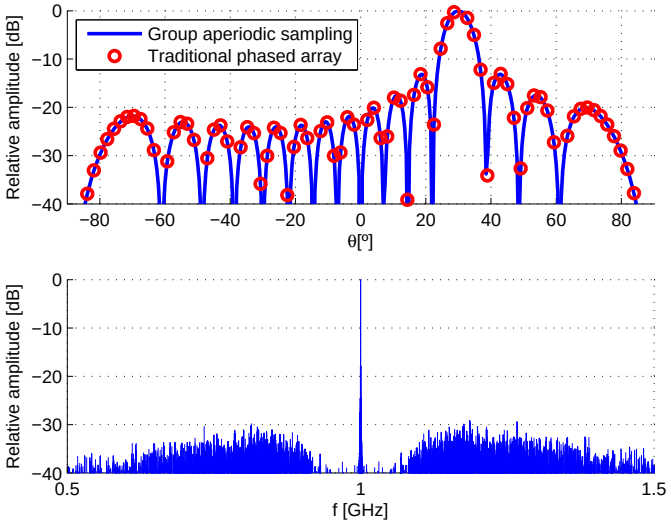

FIGURE 5.19: Received signal and radiation pattern using group aperiodic sampling after 5000 cycles

Chapter 6

Conclusions

Contents

A novel simplified sampling technique for digital phased arrays has been introduced, evaluated and simulated in this thesis. The objective of the developed technique is to reduce the generally expensive cost of phased array receivers in order to facilitate its usage in civilian applications.

After a theoretical introduction to the traditional phased array approach, a first version of the proposed technique is explained and derived analytically. The mathematical derivation shows that the proposed technique translates an angle mismatch in the space domain into a frequency shift in the spectrum domain, as the received signal is composed of an infinite set of replicas of the transmitted signal equally spaced in frequency at multiples of the aperture sampling rate. This mathematical derivation is validated by simulation, comparing the radiation pattern of the proposed technique and the traditional phased approach. All the simulations show identical results for both approaches in different combinations of number of elements and scanned angles of linear and planar arrays.

A number of elements limit given by the carrier to signal bandwidth ratio is derived using a similar method to the one used to prove Nyquist sampling theorem. Given the bandwidth limitation, the bandwidth performance of the technique has been shown by simulating the transmission of a DSB signal.

The radiation pattern study is completed by checking the effects of tapering techniques. Excitation coefficients computed using Gaussian distribution as well as Dolph Chebyshev and Taylor N-Bar have been used. The effects of applying Gaussian tapering to

the proposed technique have been simulated and compared to the traditional phased array approach, obtaining identical results for linear arrays as well as planar arrays symmetrically and asymmetrically tapered. The same equivalence is obtained for excitation coefficients obtained using well-known techniques like Dolph-Chebyshev and Taylor N-Bar. The comparative study has been performed for different number of array elements and scanned directions.

The proposed technique performance has been expanded to arbitrary array structures that include different sampling order sequences. It has been shown that the technique bandwidth, which might be too narrow for large arrays, can be enhanced by sampling the different antenna elements in an optimized order. In general terms, the optimized order will depend on the number of elements in the array as well as the scanned angle.

For small arrays ($N < 9$), the optimized order can be obtained using backtracking. For medium arrays ($9 < N < 16$), a genetic algorithm can be used. This genetic algorithm does not guarantee the optimum result, but it allows to put some harmonics below a given threshold. For large arrays ($N > 16$), it has been proved and validated by simulation that maximum delay order gives very good performance, increasing the system bandwidth up to 25 %.

Bandwidth enhancement by using non periodic sampling sequences has also been studied. As a first approach, random aperiodic structures have been simulated, showing that randomness converts secondary harmonics into distributed background noise at the cost of a radiation pattern not identical to the traditional phased array approach one. Random aperiodic sampling is improved by group aperiodic sampling, which keeps the same radiation pattern as the traditional approach and the harmonic into background noise conversion.

6.1 Future lines

Once the technique has been mathematically developed and simulated, it would be very interesting to construct a prototype that validates the research.

From the theoretical point of view, it would be interesting to improve the sampling technique in such a way that allows a reduction in the number of taken samples using some kind of simultaneous downconverting and sampling. That way, we would continue the idea of economizing the sampling technique and using only the relevant information.

Finally, it would be also interesting to perform a thorough study of the background noise produced by the aperiodic sampling sequences.

6.2 Publications

The contents of this research have been published as well as presented in a conference as listed below:

- **A novel technique for a low-cost digital phased array design**, published in *IEEE Transactions on Antennas and Propagation* [46]: Covers Chapter 3 (Introduction to the proposed technique. Mathematical derivation. Simulation results for linear and planar arrays. Bandwidth performance).
- **A new sampling scheme for digital phased arrays**, presented in *2013 International Symposium on Antennas and Propagation* [47]: Covers Chapter 3 (Introduction to the proposed technique. Monochromatic and bandwidth performance).
- **Effects of tapering in an economic sampling scheme for digital phased arrays**, sent to *Wiley Microwave and Optical Letters* [48]: Covers Chapter 4 (Gaussian, Dolph-Chebyshev and Taylor N-Bar tapering effects).
- **Phased array bandwidth enhancement using a novel sampling scheme**, sent to *IEEE Transactions on Antennas and Propagation* [49]: Covers Chapter 5 (Expansion to arbitrary arrays. Random periodic sampling. Maximum Delay sampling. Aperiodic sampling).

Appendix A

Genetic Algorithm

Contents

A.1 Introduction

A genetic algorithm is a search heuristic that imitates the natural evolution. Due to its general definition it can be used to solve many kind of different problems like engineering, economics or bioinformatics. Genetic algorithms were originally developed in the 70's. Some of the classical references for GA are [44, 50–52].

GA are based on Darwin's natural selection:

- **Selection**: Only the fittest species survive.
- **Reproduction**: New individuals are generated from two different parents.
- **Inheritance**: New individuals take traits from their parents.
- **Mutation**: New individuals may suffer from mutation to improve their characteristics.

The idea of a GA is to evolve a population from an initial set of individuals. For each generation, the best individuals are taken and descendants are generated. In order to apply this principle, two operators are defined:

- **Crossover**: Two individuals are created from two parents.
- **Mutation**: Some of the generated sons are generated looking for better performance.

Darwin's natural selection can be outlined as *"Only the fittest species survive"*. Hence, it is necessary to give a mathematical definition of fitness. This definition is known as **fitness function** and is different for each problem. The problem is completed by a mathematical model of the population that can be evaluated using the fitness function. Again, this mathematical model is likely to be different for each problem, even more than one mathematical representation is possible for the same problem.

A.2 Algorithm statement

The genetic algorithm is very simple: An initial population is evolved during a given number of generations. At the end, the best individual is selected. A scheme of a the GA is provided in Figure A.1.

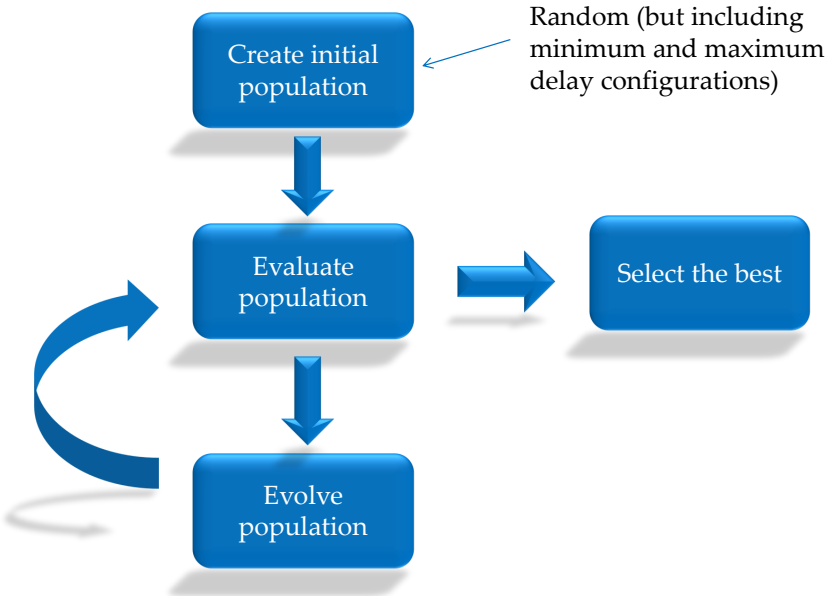

FIGURE A.1: Genetic algorithm scheme

The population evaluation and the best individual selection are based on the fitness function. On the other hand, the population evolution is based on a simple algorithm:

- Each population is made of N_i individuals.
- A percentage of elitism p_e is defined. The elite is defined as the percentage of individuals that will pass to the next generation without any change. This element assures that a generation never has a worse best individual than the previous one.
- A percentage of mutation p_m is defined. The percentage of mutation refers to the individuals that will suffer from mutation after reproduction.
- Evolve population
    1. Select $N_i(1-p_e)/2$ couples. From each couple generate two sons (crossover).
    2. Mutate $N_i \cdot p_m$ individuals.
    3. Select $N_i \cdot p_e$ from previous generation until the number of individuals is N_i.

This algorithm is common to every problem that is solvable using genetic algorithms. However, each problem will present its own essence in terms of individual representation, crossover and mutation operators and fitness function. Next section provides a description of the Genetic Algorithm used in this Thesis.

A.3 Description of the used genetic algorithm

A.3.1 Individual representation

The order sequence optimization problem can be seen as a permutation problem. As a consequence, it seems reasonable to use an array of integers as representation. The n^{th} element in the array stands for the n^{th} antenna to be sampled.

This representation can be considered as correct for two reasons:

1. All the possible individuals are represented.
2. Each combination represents one and only one individual.

A.3.2 Crossover operator

The algorithm to crossover individuals is defined as follows

1. Select two individuals to act as parents using the tournament method.
   - Randomly pick K individuals. K has been set to 4.
   - Select the two best individuals. They will serve as parents.
   - If both parents are equal, repeat the process and increase percentage of mutation.
   - If after 10 attempts no different parents are selected, generate a new random population keeping the best elements.
2. Generate a random number q between 2 and $N - 1$.
3. Take from the first parent the first q elements and complete the son by taking no repeated elements from the second parent. Repeat the process swapping parent order. This process is shown in Figure A.2.

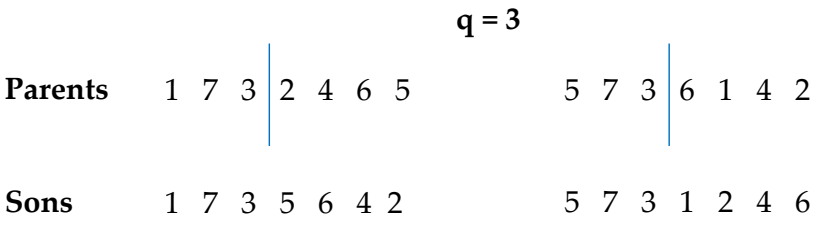

FIGURE A.2: Example of crossover. A 7 element representation has been selected. $q = 3$

It is important to keep the same number of elements in each generation. That is the reason why two individuals are selected to create two new individuals for the next generation.

A.3.3 Mutation operation

The algorithm to crossover individuals is defined as follows:

1. Select a number of gen pairs to modify.

FIGURE A.3: Example of mutation. A 7 element representation has been selected. $q = 3$

2. Swap gens as many times as required. Swapping process is shown in Figure A.3.

Based on numerous simulations it has been found that the different generations tend to stack in some fixed values for the first element. In order to create a more heterogeneous population the mutation is set to always include the first element.

It is important to compromise between the best individuals and an heterogeneous population that can lead to the optimum result.

A.3.4 Fitness function

The fitness function must measure how good is the individual. Since the optimization problem focuses in enhancing the bandwidth, it is reasonable to use as a fitness function the bandwidth after optimization, taking some threshold as acceptable interference (i.e. -30 dB).

Appendix B

Fourier Transform notes

Contents

B.1 Introduction

Along Chapters 3 and 5, Fourier Transform has been often used to study the frequency behavior of the received signal. The equations have been obtained using the pulsation notation, however, all the figures have been represented in frequency since this option is more natural and gives a more intuitive approach. The well-known result $w = 2\pi f$ has been used.

Given a generic signal $f(t)$, its Fourier Transform $F(\omega)$ is obtained according to the equation:

$$FT\left[f(t)\right] = F\left(\omega\right) = \int_{-\infty}^{\infty} f(t)e^{-j\omega t}dt \tag{B.1}$$

The inverse Fourier Transform is computed as:

$$FT^{-1}\left[F(\omega)\right] = f\left(t\right) = \frac{1}{2\pi}\int_{-\infty}^{\infty} F(\omega)e^{j\omega t}d\omega \tag{B.2}$$

This appendix is not intended to be an extensive review of the Fourier Transform but a brief guide where to consult some common steps that have been assumed as known

in the derivations. All the results presented below can be found in any signals and systems book like [53]

B.2 Used Fourier Transform properties

Given two signals $f(t)$ and $g(t)$ and their Fourier Transforms $F(\omega)$ and $G(\omega)$:

- Linearity (α and β are scalars)

$$FT\left[\alpha f(t) + \beta g(t)\right] = \alpha F(\omega) + \beta G(\omega) \tag{B.3}$$

- Translation

$$FT\left[f(t - t_0)\right] = F(\omega)e^{-j\omega t_0} \tag{B.4}$$

- Convolution

$$FT\left[f(t) * g(t)\right] = F(\omega)G(\omega) \tag{B.5}$$

- Modulation

$$FT\left[f(t)g(t)\right] = \frac{1}{2\pi}F(\omega) * G(\omega) \tag{B.6}$$

B.3 Used Fourier Transforms

Two different signals have been used: Translated delta (B.7) and a Periodic rectangular pulse (B.8)

$$FT\left[\delta(t - t_0)\right] = e^{-j\omega t_0} \tag{B.7}$$

$$FT\left[\sum_{m=-\infty}^{\infty} \Pi\left(\frac{t - mT_s}{t_s}\right)\right] = \frac{2\pi t_s}{T_s}\sum_{m=-\infty}^{\infty} sinc\left(\frac{m\pi t_s}{T_s}\right)\delta\left(\omega - \frac{2m\pi}{T_s}\right) \tag{B.8}$$

Bibliography

[1] L. Baggen, S. Holzwarth, M. Boettcher, and M. Eube, "Advances in phased array technology," in *Radar Conference, 2006. EuRAD 2006. 3rd European*, pp. 88–91.

[2] S. W. Ellingson and G. A. Hampson, "A subspace-tracking approach to interference nulling for phased array-based radio telescopes," *Antennas and Propagation, IEEE Transactions on*, vol. 50, no. 1, pp. 25–30, 2002.

[3] J. T. Mayhan, "Adaptive antenna design considerations for satellite communication antennas," *Communications, Radar and Signal Processing, IEE Proceedings F*, vol. 130, no. 1, p. 98, 1983.

[4] Y. Hwang, "Satellite antennas," *Proceedings of the IEEE*, vol. 80, no. 1, pp. 183–193, 1992.

[5] Z. Xianglin, C. Shili, Z. Zhoumo, L. Jian, J. Shijiu, and L. Zhijun, "Modelling and simulation of ultrasonic phased array in pipe flaw detection," in *Innovative Computing, Information and Control, 2006. ICICIC '06. First International Conference on*, vol. 3, pp. 145–148.

[6] S. Harput and A. Bozkurt, "Ultrasonic phased array device for acoustic imaging in air," *Sensors Journal, IEEE*, vol. 8, no. 11, pp. 1755–1762, 2008.

[7] Y. Li, M. Feuerstein, and D. Reudink, "Performance evaluation of a cellular base station multibeam antenna," *Vehicular Technology, IEEE Transactions on*, vol. 46, no. 1, pp. 1–9, 1997.

[8] S. Stapleton and G. S. Quon, "A cellular base station phased array antenna system," in *Vehicular Technology Conference, 1993., 43rd IEEE*, pp. 93–96, 1993.

[9] L. Godara, "Applications of antenna arrays to mobile communications. i. performance improvement, feasibility, and system considerations," *Proceedings of the IEEE*, vol. 85, no. 7, pp. 1031–1060, 1997.

[10] L. C. Godara, "Application of antenna arrays to mobile communications. ii. beamforming and direction-of-arrival considerations," *Proceedings of the IEEE*, vol. 85, no. 8, pp. 1195–1245, 1997.

[11] M. Johnson, "Phased-array beam steering by multiplex sampling," *Proceedings of the IEEE*, vol. 56, no. 11, pp. 1801–1811, 1968.

[12] J. D. Fredrick, W. Yuanxun, J. Seong-Sik, and T. Itoh, "A smart antenna receiver array using a single rf channel and digital beamforming," in *Microwave Symposium Digest, 2002 IEEE MTT-S International*, vol. 1, pp. 311–314.

[13] D. S. Goshi, W. Yuanxun, and T. Itoh, "A compact digital beamforming smile array for mobile communications," *Microwave Theory and Techniques, IEEE Transactions on*, vol. 52, no. 12, pp. 2732–2738, 2004.

[14] G. Krishnamurthy and K. G. Gard, "Time division multiplexing front-ends for multiantenna integrated wireless receivers," *Circuits and Systems I: Regular Papers, IEEE Transactions on*, vol. 57, no. 6, pp. 1231–1243, 2010.

[15] D. Sievenpiper, J. Schaffner, B. Loo, G. Tangonan, R. Harold, J. Pikulski, and R. Garcia, "Electronic beam steering using a varactor-tuned impedance surface," in *Antennas and Propagation Society International Symposium, 2001. IEEE*, vol. 1, pp. 174–177 vol.1.

[16] F. E. van Vliet and A. P. de Hek, "Front-end technology for phased-arrays with digital beamforming," in *Microwaves, Communications, Antennas and Electronic Systems, 2008. COMCAS 2008. IEEE International Conference on*, pp. 1–3.

[17] Z. Lou and J.-M. Jin, "Finite-element analysis of phased-array antennas," *Microwave and Optical Technology Letters*, vol. 40, no. 6, pp. 490–496, 2004.

[18] G. M. Turner and C. Christodoulou, "Fdtd analysis of phased array antennas," *Antennas and Propagation, IEEE Transactions on*, vol. 47, no. 4, pp. 661–667, 1999.

[19] Z. Yu, Z. Xun-Wang, D. G. Donoro, T. Sio-Weng, and T. K. Sarkar, "Parallelized hybrid method with higher-order mom and po for analysis of phased array antennas on electrically large platforms," *Antennas and Propagation, IEEE Transactions on*, vol. 58, no. 12, pp. 4110–4115, 2010.

[20] B. D. Van Veen and K. M. Buckley, "Beamforming: a versatile approach to spatial filtering," *ASSP Magazine, IEEE*, vol. 5, no. 2, pp. 4–24, 1988.

[21] S. Denno and T. Ohira, "Modified constant modulus algorithm for digital signal processing adaptive antennas with microwave analog beamforming," *Antennas and Propagation, IEEE Transactions on*, vol. 50, no. 6, pp. 850–857, 2002.

[22] M. Kozak and M. Karaman, "Digital phased array beamforming using single-bit delta-sigma conversion with non-uniform oversampling," *Ultrasonics, Ferroelectrics and Frequency Control, IEEE Transactions on*, vol. 48, no. 4, pp. 922–931, 2001.

[23] H. Steyskal, "Digital beamforming-an emerging technology," in *Military Communications Conference, 1988. MILCOM 88, Conference record. 21st Century Military Communications - What's Possible? 1988 IEEE*, pp. 399–403 vol.2.

[24] J. Seong-Sik, W. Yuanxun, Q. Yongxi, and T. Itoh, "A novel planar array smart antenna system with hybrid analog-digital beamforming," in *Microwave Symposium Digest, 2001 IEEE MTT-S International*, vol. 1, pp. 121–124 vol.1.

[25] K. Raczkowski, G. Mangraviti, V. Szortyka, A. Spagnolo, B. Parvais, R. Vandebriel, V. Vidojkovic, C. Soens, S. D'Amico, and P. Wambacq, "A four-path 60ghz phased-array receiver with injection-locked lo, hybrid beamforming and analog baseband section in 90nm cmos," in *Radio Frequency Integrated Circuits Symposium (RFIC), 2012 IEEE*, pp. 431–434.

[26] G. M. Rebeiz and K.-J. Koh, "Silicon rfics for phased arrays," *Microwave Magazine, IEEE*, vol. 10, no. 3, pp. 96–103, 2009.

[27] D. Parker and D. Zimmermann, "Phased arrays-part ii: implementations, applications, and future trends," *Microwave Theory and Techniques, IEEE Transactions on*, vol. 50, no. 3, pp. 688–698, 2002.

[28] S. Raman, N. Barker, and G. Rebeiz, "A w-band dielectric-lens-based integrated monopulse radar receiver," *Microwave Theory and Techniques, IEEE Transactions on*, vol. 46, no. 12, pp. 2308–2316, 1998.

[29] K. Scheir, S. Bronckers, J. Borremans, P. Wambacq, and Y. Rolain, "A 52 ghz phased-array receiver front-end in 90 nm digital cmos," *Solid-State Circuits, IEEE Journal of*, vol. 43, no. 12, pp. 2651–2659, 2008.

[30] S. P. Williams and L. E. Corey, "Mechanisms that contribute to the far-field polarization properties of phased-array antennas," in *Antennas and Propagation Society International Symposium, 1989. AP-S. Digest*, pp. 412–415 vol.1.

[31] Z. Zhao, X. Wang, K. Choi, C. Lugo, and A. T. Hunt, "Ferroelectric phase shifters at 20 and 30 ghz," *Microwave Theory and Techniques, IEEE Transactions on*, vol. 55, no. 2, pp. 430–437, 2007.

[32] T. Lambard, O. Lafond, M. Himdi, H. Jeuland, S. Bolioli, and L. Le Coq, "Ka-band phased array antenna for high-data-rate satcom," *Antennas and Wireless Propagation Letters, IEEE*, vol. 11, pp. 256–259, 2012.

[33] T. Lambard, O. Lafond, M. Himdi, H. Jeuland, and S. Bolioli, "A novel analog 360 degree phase shifter design in ku and ka bands," in *Antennas and Propagation (EuCAP), 2010 Proceedings of the Fourth European Conference on*, pp. 1–4, 2010.

[34] D. Donoho, "Compressed sensing," *Information Theory, IEEE Transactions on*, vol. 52, no. 4, pp. 1289–1306, 2006.

[35] E. J. Candès and M. B. Wakin, "An introduction to compressive sampling," *Signal Processing Magazine, IEEE*, vol. 25, no. 2, pp. 21–30, 2008.

[36] W. L. Stutzman and G. A. Thiele, *Antenna theory and design*. New York: J. Wiley, 1998.

[37] R. C. Hansen, *Phased array antennas*. Hoboken, N.J.: Wiley, 2009.

[38] A. Bhattacharyya, *Phased array antennas : Floquet analysis, synthesis, BFNs, and active array systems*. Hoboken, N.J.: Wiley-Interscience, 2006.

[39] C. L. Dolph, "A current distribution for broadside arrays which optimizes the relationship between beam width and side-lobe level," *Proceedings of the IRE*, vol. 34, no. 6, pp. 335–348, 1946.

[40] T. T. Taylor, "Design of line-source antennas for narrow beamwidth and low side lobes," *Antennas and Propagation, Transactions of the IRE Professional Group on*, vol. 3, no. 1, pp. 16–28, 1955.

[41] R. J. Mailloux, *Phased array antenna handbook*. Boston: Artech House, 1994.

[42] N. Barker and G. Rebeiz, "Distributed mems true-time delay phase shifters and wide-band switches," *Microwave Theory and Techniques, IEEE Transactions on*, vol. 46, no. 11, pp. 1881–1890, 1998.

[43] W. Ng, A. Walston, G. Tangonan, J. Lee, I. Newberg, and N. Bernstein, "The first demonstration of an optically steered microwave phased array antenna using true-time-delay," *Lightwave Technology, Journal of*, vol. 9, no. 9, pp. 1124–1131, 1991.

[44] J. H. Holland, *Adaptation in natural and artificial systems : an introductory analysis with applications to biology, control, and artificial intelligence*. Cambridge, Mass.: MIT Press, 1992.

[45] Y. M. E. Rahmat-Samii, *Electromagnetic optimization by genetic algorithms*. New York: J. Wiley, 1999.

[46] M. Manteghi and R. Blanco, "A novel technique for a low-cost digital phased array design," *Antennas and Propagation, IEEE Transactions on*, vol. 61, no. 7, pp. 3495–3501, 2013.

[47] R. Blanco and M. Manteghi, "A new sampling scheme for digital phased arrays," in *Antennas and Propagation Society International Symposium (APSURSI), 2013 IEEE*, 2013.

[48] R. Blanco and M. Manteghi, "Effects of tapering in an economic sampling scheme for digital phased arrays," *Microwave and Optical Technology Letters*, Under review.

[49] R. Blanco and M. Manteghi, "Phased array bandwidth enhancement using a novel sampling scheme," *Antennas and Propagation, IEEE Transactions on*, Under review.

[50] D. E. Goldberg, *Genetic algorithms in search, optimization, and machine learning*. Reading, Mass.: Addison-Wesley Pub. Co., 1989.

[51] J. R. Koza, *Genetic programming : on the programming of computers by means of natural selection*. Cambridge, Mass.: MIT Press, 1992.

[52] B. P. P. F. Buckles, *Genetic algorithms*. Los Alamitos, Calif: IEEE Computer Society Press, 1986.

[53] N. S. H. Oppenheim, Alan V. Willsky Alan S., *Signals and systems*. Upper Saddle River, N.J.: Prentice Hall, 1997.